Journal of Hydrology 618 (2023) 129258

Contents lists available at ScienceDirect

Journal of Hydrology

journal homepage: www.elsevier.com/locate/jhydrol

Research papers

Hydrogeochemical multi-component approach to assess fluids upwelling and mixing in shallow carbonate-evaporitic aquifers (Contursi area, southern Apennines, Italy)

Francesca Gori [a,*], Michele Paternoster [b,c], Maurizio Barbieri [d], Dario Buttitta [b,c], Antonio Caracausi [c], Fabrizio Parente [e], Attilio Sulli [e], Marco Petitta [a]

[a] Department of Earth Sciences, Sapienza University of Rome, Rome, Italy
[b] Department of Sciences, University of Basilicata, Potenza, Italy
[c] Istituto Nazionale di Geofisica e Vulcanologia, Sezione di Palermo, Palermo, Italy
[d] Department of Chemical Engineering and Environmental Materials, Sapienza University of Rome, Rome, Italy
[e] Department of Earth and Marine Sciences, University of Palermo, Palermo, Italy

ARTICLE INFO

This manuscript was handled by Corrado Corradini, Editor-in-Chief, with the assistance of Junbing Pu, Associate Editor

Keywords:
Groundwater mixing
Deep fluids
Thermal fluids
Isotopes
Hydrogeochemistry
Faults

ABSTRACT

With the aim of deepening our understanding of deep-seated fluids upwelling and mixing in large regional aquifers, we performed a hydrogeochemical study of twenty-two springs in the Contursi area (upper Sele river valley, southern Apennines) by means of the measurements of chemical-physical parameters, major ions, trace elements, and stable and radioactive isotopes. Besides, we realized two updated geo-structural cross-sections in order to reconstruct the groundwater flowpath in the study area. The hydrogeochemical composition, as well as the water temperature allow to identify-three main groups of groundwater: Cold and Low salinity Groundwater (CLGW), Intermediate Salinity Groundwater (ISGW), and Thermal Salinity Groundwater (TSGW). The CLGW group, mostly emerging at the boundary of carbonate aquifers, is characterized by alkaline earth-bicarbonate hydrofacies. Instead, ISGW and TSGW, situated in the inner zone of the valley, show gradually a hydrogeochemical evolution towards sodium-chloride type hydrofacies domain with the highest salinity value. Stable isotope ($\delta^{18}O$-δD) of CLGW reveal the local meteoric origin of groundwater, while isotopic signatures of ISGW and TSGW is associated with the deep fluids inflow. CLGW hydrogeochemistry is clearly related to dissolution of carbonate rocks. On the other hand, for ISGW and TSGW an additional contribution from evaporitic rocks is supported by saturation indices values (gypsum and anhydrite) and validated by isotopic signature of dissolved sulphate ($\delta^{34}S$-$\delta^{18}O$). The application of two models based on tritium data (i.e., the piston-flow and well-mixed reservoir) attributes longer and deeper groundwater flowpaths to TSGW. Through geothermometric calculations (e,g., K-Mg and SiO_2-quartz), the equilibrium temperature of deep fluids reservoir is also extrapolated (i.e., 75–96 °C). The results of the adopted hydrogeochemical multi-component approach allowed us to propose an interpretative model of groundwater flowpath for the Contursi area, where deep-seated tectonic discontinuities play a significant role for the upwelling of saline deep thermal fluids in shallow aquifers.

1. Introduction

The investigation of crustal-scale groundwater flow is one of the most demanding challenges for hydrogeochemistry and hydrogeological scientists. Groundwater hydrogeochemistry is the result of many simultaneous processes, involving the water–rock-gas system, that include weathering, dissolution/precipitation, ion exchange, redox reactions, sorption, gas generation and consumption, and other mechanisms (Freeze and Cherry, 1979; Matthess, 1982; Deutsch, 2020). The occurrence of these processes and their extent are strictly related to some hydrogeological factors such as (i) the nature of the aquifer system (e.g., both the lithology of host rocks, and the water-type. i.e., meteoric, marine, or magmatic), (ii) the length and depth of groundwater flowpath, (iii) the groundwater residence time, (iv) the presence and the location of tectonic features (e.g., faults and fractures) which can enhance groundwater mixing and deep fluids upwelling (Andreo et al.,

* Corresponding author at: Department of Earth Sciences, Sapienza University of Rome, Italy, Piazzale Aldo Moro 5, Rome, Italy.
E-mail address: francesca.gori@uniroma1.it (F. Gori).

https://doi.org/10.1016/j.jhydrol.2023.129258
Received 27 September 2022; Received in revised form 26 January 2023; Accepted 6 February 2023
Available online 10 February 2023

2016; Gil-Márquez et al., 2017). Therefore, water geochemistry is telling us a long and complex story that groundwater undergoes in the brittle crust (Sibson et al., 1975; Goldscheider et al., 2010; Doglioni et al., 2014; Smeraglia et al., 2018). The scale of groundwater flow both in terms of depth and width is mainly affected by the continuity of aquifer systems, hydraulic gradient between the recharge area and the discharge one, and by the presence of regional tectonic structures (Toth, 1995; De Vries and Simmers, 2002; Cook, 2003; Chen and Goldscheider, 2014). In detail, high hydraulic gradient can cause deepening of flowpaths in the aquifer that can lead groundwater up to some kilometres below the topographic surface. According to the local geothermal gradient, groundwater gets higher temperature and thus can rise convectively, mainly along faults (Minissale, 1991; Qiu et al., 2018; Yang et al., 2019). In this complex hydro-geostructural framework, the ascending of endogenous fluids (e.g., chiefly CO_2-dominant) must be considered too (Chiodini et al., 1995a, Chiodini et al., 1995b; Italiano et al., 2000; Paternoster et al., 2017; Barbieri et al., 2020; Barberio et al., 2021; Gori and Barberio, 2022). Deep fluids are generally characterized by high mineralization and abundance of gaseous content (e.g., CO_2, CH_4, Rn, He, N_2, H_2, and H_2S). These fluids are often stored in overpressurized reservoirs, upper-confined by low permeability layers, which can be connected to the surface through lithospheric fault systems (Chiodini et al., 2004; Frondini, 2008; Chiocchini et al., 2010; Trippetta et al., 2013; Smeraglia et al., 2020).

In this study, we performed a multi-component hydrogeochemical characterization of 22 springs in the Contursi area, in the inner zone of the Sele river valley (southern Apennines, Italy), where groundwater flowpaths from regional carbonate aquifers converge. Additionally, springs located along main tectonic lineaments are affected by thermalism and intense degassing with a mantle-related geochemical signatures (e.g., in Bagni di Contursi village; Panichi and Tongiorgi, 1975; Celico et al., 1979; Ghiara et al., 1994; Italiano et al., 2000; Minissale, 2004; Vannoli et al., 2021). Furthermore, recent geophysical studies furnished seismic imaging of this area from P and S waves velocity models, suggesting a fluid accumulation in a wide rock volume below the study area (Amoroso et al., 2014; Improta et al., 2014). Also, the presence of brackish and brine waters was supposed (Duchi et al., 1995; Improta et al., 2014; Amoroso et al., 2017; De Landro et al., 2022).

Owing to the various hydrogeochemical characteristics, groundwater in the Sele river valley is addressed to many different uses. For instance, fresh springs directly fed by carbonate aquifers are tapped for drinking purposes, and the mineralized and thermal ones supply spas.

The goal of this work is: a) to define water–rock interaction processes affecting the chemical composition of the investigated groundwater; b) to determine fluids origin and evolution (the mechanism of water salinization); c) to calculate the reservoir temperature using classical geothermometric approaches; d) to propose a conceptual model of fluids flowpath through the construction of two updated geological cross-sections. The results of this study may find important applications, such as exploitation of low-enthalpy geothermal resources, use of thermal waters for therapeutic purposes, and offer a relevant preliminary tool in order to define the relationship between stress field variations, pore-pressure evolution at depth in a seismically active area.

2. Geological and hydrogeological setting

The study area is located in the southern Apennines which is part of a mountain chain that develops from the Southern Abruzzi-Alto Molise region to Sicily, crossing the Calabrian arc (Malinverno and Ryan, 1986; Doglioni, 1991; Patacca and Scandone, 2007). From a geodynamic point of view, the southern Apennines are an east-verging fold-and-thrust belt related to the subduction of the Apulian lithosphere towards West (Doglioni, 1995; Faccenna et al., 2001). Starting from middle-upper Pleistocene, the axial zone of the chain raised and an extensional tectonic developed in NW-SE direction, responsible of the formation of seismogenic faults up to 15 km deep. The southern Apennines are characterized by a series of superimposed tectonic units, constituted by a deep-seated carbonate duplex system belonging to the so-called Apennine Carbonates, characterized by shallow water deformed carbonates and overlained by basinal sequences belonging to Lagonegro units (Patacca and Scandone, 2007; Ciarcia et al., 2009; Pierdominici et al., 2011; Vitale and Ciarcia, 2018). Low angle thrust faults separate the Apennine Carbonates in the hanging wall, from the Lagonegro units in the footwall. The Apennine accretionary wedge is tectonically superimposed onto the buried Apulian Platform which is characterized by the presence of folds that form hydrocarbon and CO_2 geological traps (Shiner et al., 2004) generating overpressured reservoirs. Geophysical studies carried out in this sector of Apennines (Amoroso et al., 2014; Improta et al., 2014) shed light on a diffused high V_P/v_S ratio within the fractured Apulian Platform carbonates between 5 and 10 km depth, where intense microseismicity occurs. This seismic imaging from P and S waves velocity models suggests deep-seated fluid accumulation (i.e., mixtures of brine and or CO_2) in a wide rock volume below the study area (Amoroso et al., 2017; De Landro et al., 2022).

This study focuses on the Sele river valley situated in the central portion of the southern Apennine, precisely in the Irpinia region. Commonly, the structural pattern of the upper Sele river valley has been interpreted as a NS-trending graben (Ortolani, 1975; Cotecchia, 1986; Coppola and Pescatore, 1989), where the main tectonic discontinuities border the high relief massifs made of Mesozoic carbonate rocks, located to the West and East of the Sele river valley (i.e., the Picentini Mts. and Mt. Marzano-Ogna, respectively) (Merlini and Mostardini, 1986, Wasowski et al., 2002). From a seismological standpoint, the ongoing crustal extension regime is responsible for the high seismicity of the southern Apennines. In particular, the study area represents an interesting site for seismologists since it is considered one of the areas in southern Apennines with the highest seismogenic potential (Slejko et al., 1998). It was struck by the recent strong 1980 M_w 6.9 Irpinia earthquake (Bernard and Zollo, 1989; Ascione et al., 2020) that occur few kilometres away from Contursi village. The area is currently affected by background seismicity with the most of seismic events occurring along the 1980 Irpinia deep-seated ruptures (De Matteis et al., 2012) with prevailing normal faulting focal mechanisms (Pierdominici et al., 2011).

The hydrogeological setting of the southern Apennines is characterized by *meso*-Cenozoic carbonates that act as huge karst aquifers bounded by low permeability deposits (i.e., aquitards and/or aquicludes), such as *syn*-orogenic siliciclastic marine deposits or Messinian evaporites (Boni et al., 1986; Celico et al., 2006). The upper Sele river valley is bordered to East and West by two carbonate mountain ranges: Mt. Marzano-Ogna and Picentini Mts., respectively (Fig. 1). They constitute two main aquifers of the study area because of their large volume and high hydraulic conductivity enhanced by diffuse fracturing and intense karst processes (Celico and Civita, 1976; Wasowski et al., 2002). They fed several springs located along their fault boundaries, where aquicludes of turbidite deposits are in direct contact with carbonate rocks (Budetta et al., 1988). The Picentini Mts. constitute a 600 km^2 wide large karst system and encompass four large mountain groups (Corniello et al., 2010), recognized as different hydrogeological basins. Among these basins, the Mt. Polveracchio aquifer (Fig. 1) is characterized by a complex geo-structural setting that affects groundwater flowpaths strictly constrained by tectonic discontinuities (Celico et al., 1987). Along the northern and north-eastern margin, the hydrogeological limit consists of a fault between Acerno and Calabritto localities, where the main groundwater outlet is the Acquara-Ponticchio spring (S1). Along the western margin, the boundary is represented by a fault system separating Mt. Accellica from Mt. Polveracchio. Further south, the Polveracchio basin is buffered by impermeable lithotypes of the Lagonegro units (Fig. 1; see legend: unit #7) (Corniello et al., 2010). Finally, along the eastern margin, in the upper valley of the Sele river, the boundary consists of a tectonic thrusting front, where many cold springs (i.e., S2, S3, S5, S6) are located. Through a deeper and longer circuit, groundwater feeds very mineralized springs in the inner zone of

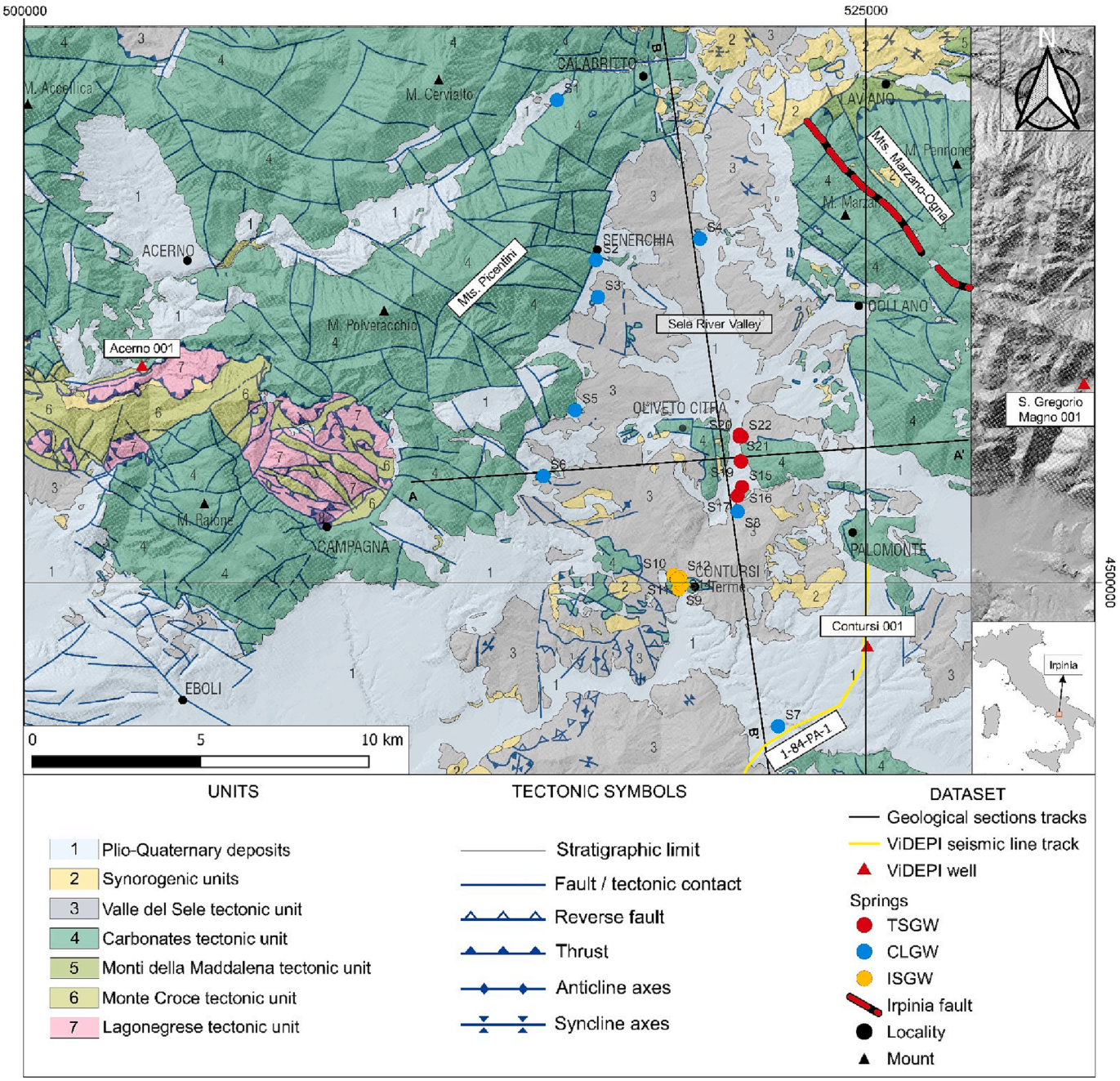

Fig. 1. Simplified tectonic map (modified after Di Nocera et al., 2016) of the Sele river valley and the dataset used for this study. In the bottom right corner, the location of the study area is reported (Irpinia region; see the red square). Lithologies of the tectonic units are described in the section 4.2.

the Sele river valley (i.e., Contursi Terme and Bagni di Contursi springs (from S15 to S22; Celico et al., 1979, Celico, 1983) by crossing carbonate substrate covered by terrigenous deposits.

3. Material and analytical Methods

3.1. Sampling, field and laboratory analysis

A sampling survey of twenty-two springs was carried out in May 2021 (Fig. 1). Water samples for major, minor and trace elements analyses were filtered with 0.45 μm membrane filters and, to keep metals in solution, the latter were acidified on-site (with ultrapure HNO_3 to pH = 2). Water samples for isotopic analyses ($\delta^{18}O$-H_2O, δD-H_2O, ^3H-H_2O, $\delta^{34}S$-SO_4, and $\delta^{18}O$-SO_4) were collected without treatments. They were sampled into high-density polyethylene bottles and stored at low temperatures in ice-filled fridge boxes to avoid alterations of chemical components.

Electrical conductivity (EC) measured at 25 °C, Temperature (T), and pH were directly measured in situ using the multiparametric probe WTW Multi 3420 with accuracies of 1 μS/cm, 0.1 °C, and 0.01 pH unit, respectively.

Anions and cations were determined by ion chromatography at the Geochemistry Laboratory of the Department of Earth Sciences at Sapienza University of Rome. Chromatographs Dionex ICS 5000, and Dionex ICS 1100 were used to analyse anions (F^-, Cl^-, SO_4^{2-}, and NO_3^-), and cations (Ca^{2+}, Mg^{2+}, Na^+, and K^+), respectively. Bicarbonate ions were measured by titration with 0.05 N HCl solution as titrating agent and methyl orange as indicator. Ionic-balance error checked on each sample was within ± 5 % (Baird et al., 2017). Dissolved SiO_2 was measured by VIS spectrophotometry upon reaction with ammonium molybdate in

acid media (and treatment with oxalic acid) to form a yellow silicomolybdate complex, whose absorbance was read at 410 nm (Nollet, 2007).

Samples for trace elements were analysed using an ICP-MS spectrometer (X Series 2 Thermo Fisher Scientific Waltham, MA, USA). Blanks, standard solutions, and sample dilutions were prepared by using ultrapure water (Millipore, Milli-Q, 16 MW cm), and an internal standard (Rh) was added to correct the ICP-MS instrumental drift. The analytical accuracy of this method ranges between 2 % and 5 %.

Measurements of the water stable isotope ratios ($\delta^{18}O$ and δD), and the sulphur and oxygen isotopic composition in dissolved sulphate ($\delta^{34}S$-SO_4 and $\delta^{18}O$-SO_4) are expressed in terms of delta units (‰) units relative to the Vienna Standard Mean Ocean Water (V-SMOW) and Vienna Canyon Diablo Troilite (V-CDT) standards, respectively. Tritium (^3H) content was determined by an electrolytic enrichment and liquid scintillation counting method, and it is reported in TU (Tritium Unit). These analyses were performed only on some springs (i.e., S2, S4, S7, S9, S10, S16, S17, S18, S21) at IT2E Isotope Tracer Technologies Europe Srl in Milan (Italy).

The speciation software PHREEQC Interactive 3.6.2 (Parkhurst and Appelo, 2013) was used to calculate Saturation Index (S.I.).

3.2. Calculation of mean residence time of groundwater

Tritium (^3H) is a natural radioactive isotope of hydrogen (its short half-life is of 12.32 years) that can be used as a tracer for determining the groundwater age. Due to the increase and decrease of this radionuclide in rainwater during atmospheric nuclear-weapons testing in the 1945–1963 s, it is often used to differentiate groundwater recharged before and after the early 1950 s (McMahon, 2012). Groundwater age is useful to estimate recharge rates (Wang et al., 2008), to propose hydrogeochemistry models on the fluid circulation (Sanford, 2011, Apollaro et al, 2015) and to infer information on the vulnerability of aquifers to contamination by anthropogenic activities at the land surface (Raco et al., 2022). The dating of groundwater assumes that the tritium activity at the time of recharge is known and that the measured value in water sample corresponds only to the radioactive decay. The estimation of the mean residence time of groundwater was obtained by adopting two end-member models, i.e., the piston-flow and the well-mixed reservoir. The piston-flow model assumes absence of mixing along the whole water flowpath, from the recharge area to discharge one. Contrarily, the well-mixed reservoir model assumes complete mixing between the water entering the reservoir and the water already stored into it (Shevenell and Goff, 1995; Apollaro et al., 2015; Apollaro et al., 2016). To link tritium content of groundwater to its mean residence time, it was necessary to take into account tritium data of local rainwaters from the IAEA-WMO stations (IAEA/WMO, 2013) and from the Global Network of Isotopes in Precipitation (GNIP) in Italy and Europe. About 2000 values of rainwaters from 1953 to 2019 have been used in order to define tritium contents as a function of time. The dataset shows a sudden increase in tritium values in 1961–1963 and then a gradual decrease until reaching constant values (around 8.5 Tritium Unit) in recent years (tritium-time plot is reported in Fig. S1) As described by Apollaro et al. (2015, 2016), the required input functions, calculated in the dataset in different number of segments, have been defined and applied for two different models (the piston-flow and the well-mixed reservoir) in the equations proposed by Shevenell and Goff (1995), linking the output tritium concentration at time t to the mean residence time of water in the geothermal reservoir.

3.3. Geothermometers

The classical method used to calculate the reservoir temperature is chemical geothermometry consisting of the use of different empiric or experimental calibrations based on temperature dependent heterogeneous chemical reactions. Many geothermometric techniques have been proposed through the years for different geochemical and geological settings (Fournier, 1977; Fournier and Potter, 1979; Fouillac and Michard, 1981; Arnórsson et al., 1983; Marini et al., 1986; Giggenbach, 1988; Chiodini et al., 1995a, Chiodini et al., 1995b; Battistel et al., 2014). It is known that chemical geothermometers are based on some theoretical assumptions: (i) water is in equilibrium with host rocks, as such water is saturated by the mineral phases governing the geothermometer, and (ii) the waters neither re-equilibrate nor mix with shallow circulating fluids during the ascent towards the surface. The silica geothermometers (SiO_2- chalcedony, and SiO_2-quartz; Truesdell, 1976; Fournier, 1977), and cation geothermometers (K-Mg; Giggenbach, 1988; Fournier, 1979; Fournier and Truesdell, 1973) were employed in this study.

3.4. Geological cross-section construction

To achieve the goal of this study, also two orthogonal schematic geological sections were made in order to reconstruct the fluids flowpaths down to 5 km depth below the surface. Both the cross sections fall within the Sele river valley: the first one is a W-E section (A-A') and the second one is a N—S section (B-B') (see Fig. 1). These sections have been realized by using as reference the "Foglio 468 – Eboli", which is a geological map of the CARG (CARtografia Geologica) project, on a scale of 1:50.000 (Fig. 1 shows the tectonic scheme obtained from the above-mentioned map). Regarding the reference elevation model, the DEM provided by the TINITALY portal (Tarquini et al., 2007) was used. Based on ViDEPI database, wells "Acerno 001", "Contursi 001", and "S. Gregorio Magno 001" were studied in order to calibrate the geological sections. All the data were imported and elaborated both in QGIS (v. 3.22.5) and in MOVE™ software (v. 2022.1).

4. Results

4.1. Hydrogeochemical characterization

The chemical-physical parameters, major ions, minor and trace elements, saturation indices, and isotopic data ($\delta^{18}O$-H_2O, δD-H_2O, ^3H-H_2O, $\delta^{34}S$-SO_4, and $\delta^{18}O$-SO_4) are listed in Table 1, Table 2, and Table 3.

According to the EC and T values, three main groups can be clearly recognized (see Fig. 3). Also, the multivariate statistical approach of Principal Component Analyses (PCA) was performed (Maćkiewicz and Ratajczak, 1993) using R software to support and validate the hydrogeochemical classification of samples based on chemical compositional similarities. The first two principal component resolve 96.5 % of the total data variance (see Fig. S2).

A first group, represented by Cold and Low salinity Groundwater (hereafter CLGW) includes samples from S1 to S8 (see Table 1). These waters have the lowest EC (≤700 μS/cm) and T values (from 7.8 to 14.3 °C). The pH values are alkaline between 7.2 and 8.4, and these waters are in oxidizing condition (average value of 247 mV). They show a Ca-Mg-HCO_3 hydrofacies (Fig. 4). A second group with Intermediate Salinity Groundwater (hereafter ISGW) includes samples from S9 to S14 (see Table 1). They show T values between 13.8 and 18.5 °C, EC values from 1090 to 1981 μS/cm. The pH values are slightly acidic (from 6.0 to 6.8), while Eh values are between –197 and 229 mV. ISGW belongs to Ca-Mg-HCO_3 hydrofacies like CLGW. A third group of Thermal and Saline Groundwater (hereafter TSGW) includes samples from S15 to S22 (see Table 1). In detail, TSGW group is brackish-type water, according to the classification of Drever (1997), having EC values from 2560 to 6470 μS/cm. The latter are thermal with T values between 25 and 47 °C, slightly acidic (pH values from 6.2 to 6.4) and have negative Eh values (up to –285 mV). Furthermore, they are characterized by a Na-HCO_3-Cl composition (Fig. 4) and show a marked enrichment in sulphate respect to other groups (Table 1). These waters show a bubbling gas phase and have high dissolved CO_2 values too (Italiano et al., 2000). NO_3 values are generally very low, at times ranging from below the detection limit,

Table 1
Chemical-physical parameters, and major ions composition of groundwater from the study area are shown (numbers of springs correspond to the sites shown in Fig. 1).

Spring	Location		Chemical-physical parameters and Major Ions											
	Latitude UTM 33T	Longitude UTM 33T	T °C	pH	EC µS/cm	Eh mV	Ca mg/L	Mg mg/L	Na mg/L	K mg/L	Cl mg/L	SO4 mg/L	HCO3 mg/L	F mg/L
S1	4514317.88	515823.1	7.8	7.8	354	272.4	78.7	7.2	4.0	1.0	5.7	3.2	250.2	0.07
S2	4509575.13	516,989	7.9	7.7	300	252.7	55.2	10.2	3.2	1.0	5.1	2.4	228.8	0.05
S3	4508475.04	517046.1	9.7	8.4	298	206.5	48.1	12.2	3.9	1.0	5.7	3.0	213.6	0.05
S4	4510201.66	520069.8	10.5	7.4	518	298.7	92.5	14.8	5.9	1.4	7.9	5.7	357.0	0.12
S5	4505117.4	516,361	10.1	7.8	352	301.8	74.1	8.6	4.9	1.0	6.6	3.5	247.1	0.08
S6	4503164.03	515417.3	12.1	7.5	398	178.3	97.0	1.9	7.6	1.3	9.5	5.3	274.6	0.07
S7	4495742.24	522392.7	12.8	7.2	664	299.01	121.2	17.5	12.9	2.3	18.5	11.9	433.2	0.22
S8	4502107.15	521191.1	14.3	7.5	613	166.3	132.6	5.5	13.5	0.9	19.4	14.9	387.5	0.16
S9	4499811.48	519441.4	14.1	6.5	1090	85.8	243.4	22.8	21.5	3.9	28.7	16.1	771.9	0.25
S10	4500221.41	519281.3	17.3	6.1	1981	−197.3	454.3	47.8	88.1	9.8	102.1	40.0	1388.2	0.40
S11	4500115.23	519383.4	14.7	6.5	1435	228.9	329.9	31.0	41.4	5.8	52.5	25.9	1000.7	0.24
S12	4500159.22	519482.9	18.5	6.0	1924	−147.8	407.5	49.6	112.3	12.2	136.8	52.0	1266.2	0.27
S13	4500097.7	519399.5	14.4	6.6	1298	213.6	295.4	25.7	30.3	4.9	40.3	20.8	909.2	0.24
S14	4499940.76	519529.2	13.8	6.8	1054	198	239.6	25.4	21.9	4.1	28.9	16.4	765.8	0.25
S15	4502838.02	521319.4	26.4	6.3	2570	−224.5	427.9	40.4	206.0	31.4	252.1	162.7	1385.2	1.12
S16	4502837.92	521317.3	26.4	6.3	2560	−219.2	440.4	43.1	210.0	31.0	320.6	202.3	1434.0	1.51
S17	4502573.69	521,185	24.8	6.2	2770	−197.5	455.4	44.5	223.9	30.3	397.0	238.1	1446.2	1.15
S18	4503593.2	521292.7	36.8	6.2	4460	−273.2	248.7	94.3	438.5	67.8	795.4	266.3	1434.0	0.61
S19	4503601.13	521280.3	37.5	6.3	4640	−258.5	608.9	78.4	444.5	56.2	769.4	254.6	2224.2	1.49
S20	4504333.49	521,240	34.3	6.2	5240	−273.9	639.1	85.5	617.4	73.7	1027.1	479.5	2196.7	1.84
S21	4504385.25	521241.9	46.7	6.4	6380	−285	288.4	132.9	995.8	115.7	1694.0	321.9	1592.6	1.39
S22	4504331.3	521308.4	47	6.4	6470	−263	598.2	127.3	1063.0	113.4	1485.9	389.3	2349.3	1.69

Table 2
Trace elements concentrations, stable and radioactive isotopic contents of groundwater from the study area are shown (numbers of springs correspond to the sites shown in Fig. 1).

Minor elements and Isotopes											
Spring	Li	B	Rb	Sr	Cs	Ba	δ^2H-H_2O	$\delta^{18}O$-H_2O	^3H	$\delta^{18}O$-SO_4	$\delta^{34}S$-SO_4
	µg/L	µg/L	µg/L	µg/L	µg/L	µg/L	‰ V-SMOW	‰ V-SMOW	TU	‰ V-SMOW	‰ V-CDT
S1	3.1	<0.002	3.9	33.8	1.6	8.2					
S2	<0.002	<0.002	2.0	29.9	0.04	5.2	−50.4	−8.5	1.4		
S3	0.2	<0.002	1.3	33.7	0.02	5.9					
S4	4.3	<0.002	1.8	114.9	0.04	13.2	−47.2	−8.0	1.0		
S5	<0.002	<0.002	1.8	32.9	0.03	5.6					
S6	<0.002	<0.002	2.5	81.4	0.01	9.6					
S7	24.3	132.5	2.6	191.7	0.7	13.8	−46.4	−7.8	2.2		
S8	3.5	21.8	0.5	721.8	0.04	30					
S9	94.4	688.7	5.6	359.1	2.6	13.9	−44.6	−7.5	2.2	6.8	9.7
S10	576.9	3545	18.6	902.0	10.4	22.2	−43.9	−7.4	1.7	8.4	18.0
S11	302.7	1818	13.6	566.1	11.9	21.3					
S12	779.9	4925	20.7	984	10.1	29.1					
S13	263.3	1871	9.4	516.4	4.9	15.8					
S14	108.7	1067	6.4	380.5	2.7	15.0					
S15	1602	9107	50.8	2331.0	57.7	53.4					
S16	1574	9176	52.7	2425.0	60.6	55.4	−38.4	−6.3	2.3	7.3	9.9
S17	1730	10,620	103.3	2524.0	80.9	46.6	−39.0	−6.4	1.3	5.3	10.7
S18	3434	20,470	203.1	4867.0	149.3	67.0	−42.1	−6.4	1.1	8.2	16.8
S19	3846	23,230	219.1	5247.0	162.1	71.8					
S20	4737	28,360	288.5	6810.0	214.5	78.2					
S21	6588	40,650	409.5	9130.0	313.6	102.9	−48.1	−6.3	1.4	6.7	21.9
S22	6342	38,640	387.5	8936.0	293.2	102.5					

from 0.18 to 4.15 mg/L (S20) and did not show significant differences among the three groups. Among minor and trace elements (F, Li, B, Rb, Sr, Cs, SiO_2, and Ba), TSGW show the highest concentrations, up to three orders of magnitude higher than CLGW and ISGW groups. The $\delta^{18}O$-H_2O and δD-H_2O values measured in nine samples (three of CLGW group, two of ISGW group and four of TSGW group, Table 2) range from − 8.5 to − 6.3 ‰, and from − 50 to − 38 ‰, respectively. The $\delta^{34}S$-SO_4 and $\delta^{18}O$-SO_4 values measured in six samples, belonging to ISGW and TSGW groups, show the following range values: from 5.3 to 8.4 and, from 9.7 to 21.9 for $\delta^{18}O$ and for $\delta^{34}S$, respectively. Finally, tritium content is between 1 and 2.3 TU (see Table 2) measured in nine water samples.

4.2. Geo-structural interpretation

With the aim of furnishing a model for groundwater and deep fluids flowpaths, and to reconstruct the geological scheme of the Sele river Valley, we realized two schematic geological cross-sections both longitudinally and transversally with respect to the location of thermal springs and to the vergence of the Apennines fold-and-thrust belt, as well as a stratigraphic column down to a depth of about 5 km (Fig. 2).

In the central part of the A-A' section (Fig. 2), the so-called Valle del Sele tectonic unit results to be the geometrically highest unit in the area, overlying the Carbonate tectonic unit, with a maximum thickness of about 400 m. The Valle del Sale tectonic unit is characterized, from

Table 3
Calculated saturation indices of groundwater from the study area are shown (numbers of springs correspond to the sites shown in Fig. 1).

Saturation Indices				
Spring	Anhydrite	Calcite	Dolomite	Gypsum
S1	−3.47	0.46	−0.04	−2.96
S2	−3.7	0.24	−0.17	−3.2
S3	−3.66	0.84	1.21	−3.18
S4	−3.17	0.29	−0.09	−2.7
S5	−3.43	0.43	0.05	−2.95
S6	−3.14	0.35	−0.85	−2.69
S7	−2.77	0.32	−0.02	−2.33
S8	−2.61	0.66	0.14	−2.18
S9	−2.48	0.1	−0.64	−2.05
S10	−1.97	0.13	−0.47	−1.58
S11	−2.22	0.28	−0.27	−1.8
S12	−1.88	0.01	−0.63	−1.5
S13	−2.33	0.29	−0.28	−1.9
S14	−2.48	0.38	−0.02	−2.05
S15	−1.34	0.39	0.12	−1.05
S16	−1.24	0.4	0.17	−0.96
S17	−1.19	0.39	0.12	−0.88
S18	−1.31	0.21	0.46	−1.13
S19	−1.06	0.82	1.23	−0.89
S20	−0.83	0.67	0.91	−0.63
S21	−1.19	0.57	1.31	−1.12
S22	−0.89	1	1.83	−0.81

bottom to top, by the presence of clayey units interspersed with marly limestones, clayey-limestones, and arenaceous-marl (Di Nocera et al., 2016). The lower unit is the so-called Carbonate tectonic unit with a maximum thickness of about 3500 m. It outcrops in Picentini Mts. and in Mt. Castello (the western and eastern part of the A-A' cross section, respectively), and also in the structural highs of Oliveto Citra and Mt. Pruno. It consists of Mesozoic carbonates deposited in an interval between the Triassic and the Cretaceous and generated in a transition sector between the carbonate shelf edge and the Lagonegro Basin (Di Nocera et al., 2016). At the bottom of the carbonates, there are dolomitic successions. The Picentini Mts. were generated by the E-verging thrust front, while the back thrust and the respective splays, that dissects the Carbonate units in the eastern part, are responsible for the presence of the Oliveto Citra and Mt. Pruno highs (see Fig. 2). These tectonic structures have been also recognized in the ViDEPI seismic line "1–84-PA-1" (see location in Fig. 1). The unresolved western part of the A-A' section is due to the uncertainty given by the huge vertical displacement that involved the Lagonegrese tectonic unit (Fig. 2).

In the B-B' section, both the Valle del Sele tectonic unit and the Carbonate tectonic unit are covered, at times, by the synorogenic unit in erosive and disconformable contact (Fig. 2). In the northern part of the section, a lateral ramp, tectonically underlying to the Carbonate tectonic unit, is constituted by the carbonates of Monti della Maddalena tectonic unit (Di Nocera et al., 2016) with a maximum thickness of about 2000 m (Fig. 2). At the bottom, it is constituted by the presence of an intensely fractured dolomitic succession (from Upper Triassic to Lower Jurassic). At the top, it consists of a carbonate platform succession (from the Lower Jurassic to the Upper Miocene). The Lagonegrese tectonic unit is mainly represented by Mesozoic clayey deposits of deep-sea environment, and, at the top, by flysch deposits. In this area, the maximum thickness of the Lagonegrese tectonic unit is about 2000 m. The tectonic contact between the Lagonegrese unit and the Apulian carbonates is found at a depth of 4286 m in the "Acerno 001" well (see location in Fig. 1). This well falls in the Campagna tectonic window, which testifies the presence of a tectonic doubling of the Lagonegrese units (Patacca, 2007) that could justify the shallow depth of these units in the western part of the cross section. The doubling of the Lagonegrese units is also due to the sandwiching of the Mt. Croce tectonic unit, which outcrops in the western part of the study area (Fig. 1), but it is not in the area of sampling and is not crossed by the geological sections. The presence of the evaporitic Messinian Gessoso-Solfifera Formation, mainly constituted by gypsum and clays, with a thickness of about 80 m, is also reported. The geometrically deepest tectonic unit recognizable in the area is represented by the Apulian carbonates up to, at least, 5 km in depth. It is constituted by shallow water Mesozoic-Tertiary platform carbonates. As shown in both sections, regarding the tectonic discontinuities, a deep normal fault crosses both the Messinian Gessoso-Solfifera Formation and the Apulian carbonates. It is supposed to be responsible for playing a crucial role in the uprising of deep fluids towards the surface in the area of Bagni di Contursi (Fig. 2). Overall, carbonate units are the most common in the area and represent both the edge and the central part of the carbonate platform. At the bottom of these units, intensely fractured dolomitic successions are present and classified as cataclasites and ultracataclasites (Di Nocera et al., 2016). It is worthy of note that Montanari et al. (2017) analyzed drill-stem-tests performed in Mesozoic carbonate units, whose physical features are comparable with the ones of the Sele River valley, and they also measured porosity and permeability values, over 6 km depth. On fine-grained dolostones and vuggy dolomicrites, they measured an average permeability $<1.0 \cdot 10^{-18}$ m^2 and equal to $7.7 \cdot 10^{-13}$ m^2, respectively. In carbonate units, permeability varies from $1.9 \cdot 10^{-16}$ m^2 to $1.2 \cdot 10^{-13}$ m^2. Besides, taking into account the P waves velocity provided by Valoroso et al. (2011), the density of the main

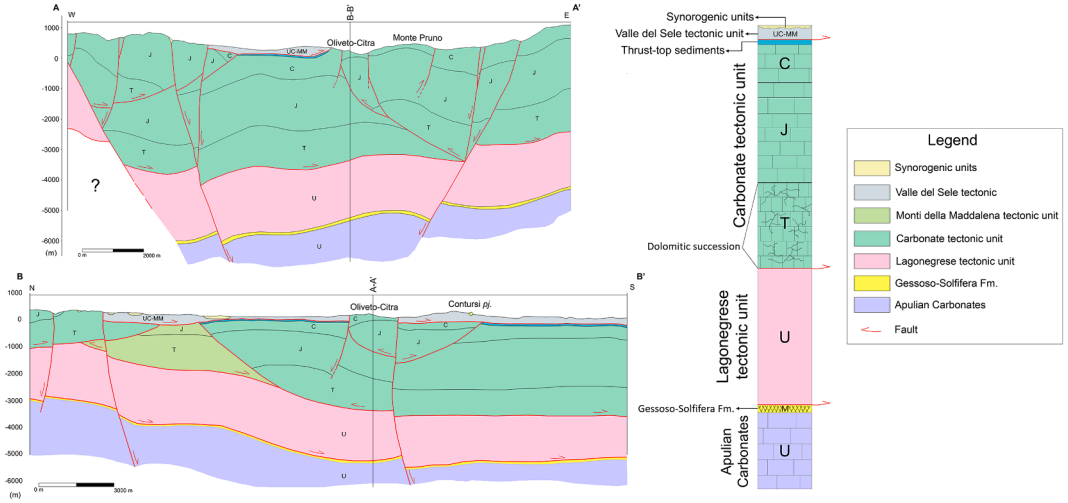

Fig. 2. Schematic cross sections (A-A' and B-B'; see Fig. 1 for location) and the lithostratigraphic column. UC-MM: Upper Cetaceous-Middle Miocene; C: Cretaceous; J: Jurassic; T: Triassic; M: Messinian; U: Undefined age.

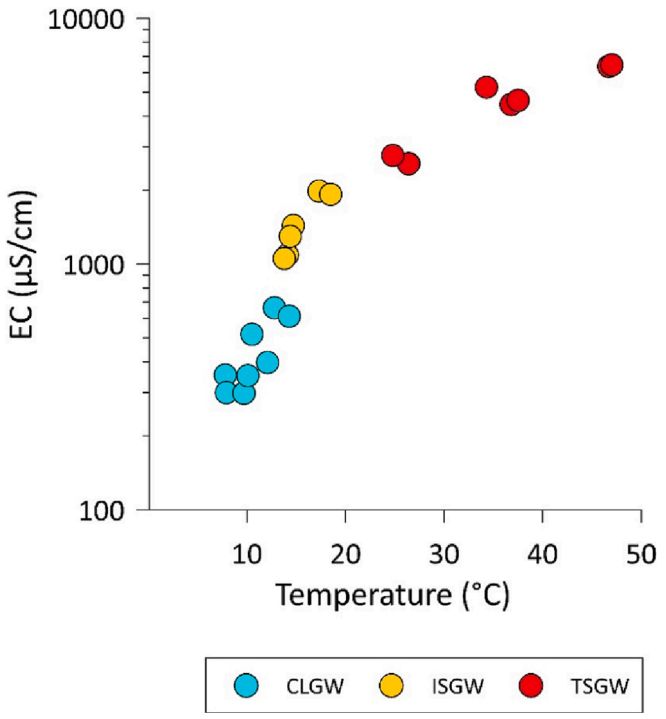

Fig. 3. Electrical conductivity (µS/cm) vs temperature (°C). Three groups of groundwater (i.e., CLGW, ISGW, and TSGW) are identified and displayed with different colours.

tectonic units was calculated and also the lithostatic pressure at 5 km depth was set at about 1.3 Kbar.

5. Discussion

5.1. Water-Rock interaction processes

The Langelier-Ludwig diagram (Fig. 4) clarifies that T and EC increase (Fig. 3) is related to a gradual enrichment of the Cl-SO_4 and Na contents, starting from Ca(Mg)–HCO_3 composition of cold samples (CLGW type) up to Na-HCO_3-Cl composition of thermal samples (TSGW type). In this latter hydrogeochemical facies, the composition of brine waters both in the Apennine context (Toscani et al., 2007; Boschetti et al., 2011a; Boschetti et al., 2011b), and in the volcanic/geothermal one (Minissale et al., 2016) were reported (Fig. 4). The separation between CLGW and TSGW groups is well-marked, while most springs of ISGW group show an intermediate composition, suggesting the presence of mixing processes between the cold end-member and the thermal one.

To evaluate both the role of the lithologies involved in the main geochemical processes, and the related mixing process, the relationships between the main solutes have been investigated. The Ca/(Ca + Mg) ratios have been plotted against $HCO_3/(HCO_3 + SO_4)$ ratios (Fig. 5) in order to verify if the aquifers are dominated by carbonate-evaporite rocks. The CLGW and ISGW groups fall along calcite and dolomite dissolution line, indicating that the dissolution of carbonate rocks (mainly calcite) is the main process. Conversely, TSGW is more shifted towards an anhydrite end-member than CLGW. The relative increase in Mg^{2+} goes on with an increase of SO_4^{2-}, suggesting that TSGW are affected by dedolomitization driven by dissolution of gypsum or anhydrite. This process is quite common in aquifers containing dolostones associated with gypsiferous layers (Capaccioni et al., 2001; Appelo and Postma, 2005; Ma et al., 2011; Capecchiacci et al., 2015). The gypsum dissolution determines an increase in Ca^{2+} which in turn allows calcite to precipitate. Consequently, the decrease in CO_3^{2-} causes the dolomite dissolution and the Mg^{2+} increase in solution (Gil-Márquez et al., 2017; Apollaro et al., 2020). These constraints are confirmed by saturation indices of calcite, dolomite and gypsum, representative of the carbonate and evaporite components (Table 2). Fig. 6a shows that CLGW and ISGW groups are in equilibrium with calcite, slightly undersaturated in dolomite, and strongly undersaturated with respect to gypsum. TSGW is in equilibrium with calcite, supersaturated or in equilibrium with dolomite, and slightly undersaturated with a trend towards saturation with respect to gypsum (Fig. 6b).

The mixing processes between cold end-member and thermal one is also well represented by Na-Cl diagram (see Fig. S3). All investigated waters align along the Na/Cl ratio ~ 1 with TSGW having higher values than ISGW and CLGW. For the latter ones, the Na/Cl ratio is linked to seawater spray while for thermal waters (TSGW), it can be associated to deep fluids uprising produced by halite dissolution from evaporitic layers.

TSGW shows also high F^- concentrations (from 0.61 to 1.84 mg/L) that are probably linked to the presence of fluorine-containing minerals, such as fluorapatite, fluorite and phlogopite in the lithology through which the water flows. The precipitation of calcite and subordinately dolomite could cause the removal of Ca^{2+} and enhance fluorite dissolution and F^- enrichment, as proposed by Apollaro et al. (2020) for carbonate aquifers.

In the TSGW, the high B concentrations and the positive correlation with Cl^- content (conservative element) supports the occurrence of evaporitic-water interaction process, since this element is typically enriched in evaporite sequences (Battistel et al., 2016; Holser, 2018). Similarly to B, also Li and Rb show a good positive correlation with Cl^- (high Pearson's "r" correlation coefficient greater than 0.9; see Fig. S4 and Table S1) suggesting a contribution from water-rock interaction (Wang et al., 2019).

5.2. Oxygen and hydrogen isotope composition

The δD and $\delta^{18}O$ values are displayed in Fig. 7, together with Southern Italy Meteoric Water Line (SIML; Longinelli and Selmo, 2003) and Global Meteoric Water Line (GMWL; Clark and Fritz, 2013). CLGW is enriched in lighter isotopes and falls on SIML representing the shallow component (i.e., the current meteoric recharge of the aquifer). Similar to CLGW type, ISGW samples fall on meteoric water line and are located between the shallow cold end-member (CLGW type) and the inflowing thermal and brackish fluids (TSGW type) with oxygen isotopic signature more enriched in heavy isotopes. TSGW type has a narrow range of $\delta^{18}O$ values (from –6.38 ‰ to –6.30 ‰), and conversely a wide variability for δD. They move away from SIML with a positive $\delta^{18}O$-shift, more marked for S18 and S21 showing the highest T and salinity value. Generally, saline waters (brackish, brine, connate, formation water, metamorphic water, etc.) fall on the right of the local meteoric water line, though scattered with an increase in both $\delta^{18}O$ and δD values with increasing salinity and T (Kharaka and Hanor, 2003; Hoefs, 2009; Toscani et al. 2007; Boschetti et al., 2011a; Boschetti et al., 2011b; Sharp, 2017), and their origin cannot be related to present-day precipitation. From an isotopic point of view, the composition of TSGW may be interpreted as a mixture between brine-type waters, originated from deep aquifer flowing upward, and cold water. In order to verify this hypothesis, the $\delta^{18}O$ values are plotted against Cl^- contents together with mixing lines between cold water (representing local meteoric water line) and average values of brine-type from literature (Fig. 8). For shallow end-member we used the average values of cold water (Cl = 10.4 mg/L and $\delta^{18}O$ = –8.09 ‰) while for brine end-member Cl^- contents between 70 and 120 g/L and $\delta^{18}O$ value of + 5 ‰ (Toscani et al., 2007; Boschetti et al., 2011a; Boschetti et al., 2011b; Yan et al., 2013) has been taken into account. Thermal waters do not fall on the mixing lines, showed an enrichment in heavy oxygen isotope linked probably to secondary processes responsible for the modification of the chemical and isotopic composition.

Additionally, thermal waters in Contursi area are characterized by bubbling gases with high CO_2 content (Duchi et al., 1995; Italiano et al.,

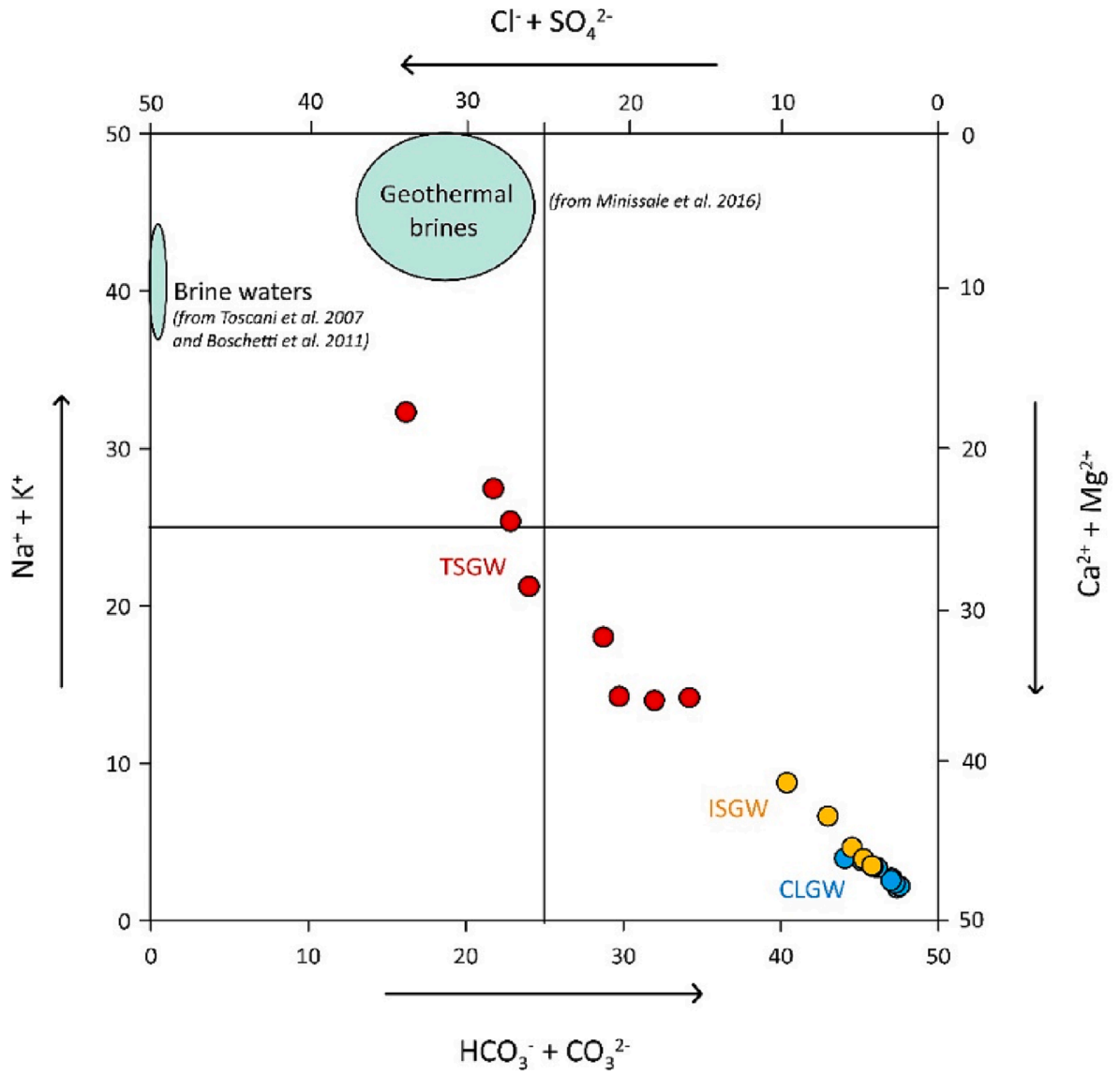

Fig. 4. Langelier-Ludwig diagram (Langelier and Ludwig, 1942) for groundwater samples from the Sele river valley. Most of samples are enriched in bicarbonate and calcium-magnesium ions (Ca-Mg-HCO_3 hydrofacies). Only mineralized springs of the Contursi area are included in the sodium-chloride waters domain (Na-Cl hydrofacies). In detail, Cold Low salinity Groundwater (CLGW), Intermediate Salinity Groundwater (ISGW), and Thermal Saline Groundwater (TSGW) are displayed with cyan, yellow, and red circles, respectively; Literature data of brine waters and geothermal brines are also displayed (Toscani et al., 2007; Boschetti et al., 2011; Minissale et al., 2016).

2000; Minissale, 2004). It is known that for CO_2-rich waters various natural processes may deviate the $\delta^{18}O$ e δD values in reservoir waters from equilibrium values on the meteoric water line. Generally, ^{18}O enrichment, with no change in the hydrogen isotope ratio, has been associated with oxygen isotope exchange with bedrock minerals or water-steam separation in geothermal conditions (Clayton and Steiner, 1975; Matsuhisa et al., 1979; Giggenbach, 1992), while ^{18}O depletion is proposed to be due to CO_2-water interaction at lower temperatures. Recently, Karolite et al. (2017) have verified that for CO_2-rich springs the equilibration with CO_2-dominat gas can result in ^{18}O enrichment and depletion in waters and therefore geothermal conditions are not necessary to produce ^{18}O-enriched waters. The ^{18}O enrichment is facilitated if the starting $\delta^{18}O$ value of CO_2 is significantly higher than that of the water and if high gas–water ratios are present (Karolyte et al., 2017). Our samples show these conditions linked to CO_2, nevertheless thermal waters are characterized from a big range of δD values, too. The δD enrichment without an effect on $\delta^{18}O$ can be justified from fractionation between degassing H_2, H_2S, CH_4, and water in active magmatic systems (Richet et al., 1977). However, the chemical geothermometers indicate roughly that Contursi area is characterized by a low temperature geothermal system, not comparable to an active magmatic one. Alternatively, it is possible that the big range of δD values can be attributed to recharge in past at different temperatures, higher than the current one. A further explanation for this variability of isotopic data (positive $\delta^{18}O$-shift and the value range in δD) can be linked to evaporative processes. In fact, during evaporation the lighter isotopes (^{16}O and ^{1}H) enter the vapour phase, and consequently water vapour is depleted in ^{18}O and ^{2}H, whereas the remaining water is enriched in both heavier isotopes (^{18}O and ^{2}H). The d-excess ($d = \delta D - 8\ \delta^{18}O$) is an important parameter for evaluating the effect of evaporation (Hoefs, 2009) and its value decreases during the evaporations process. The deuterium excesses of investigated groundwater, calculated using the SIML, range from 11.8 ‰ (S2) to – 2.05 ‰ (S21). Plotting the d-excess vs EC values (Fig. 9), it is possible to verify if the evaporation process is occurred. CLGW and ISGW are located along the dissolution line, while TSGW shows a negative correlation falling into the area linked to evaporative

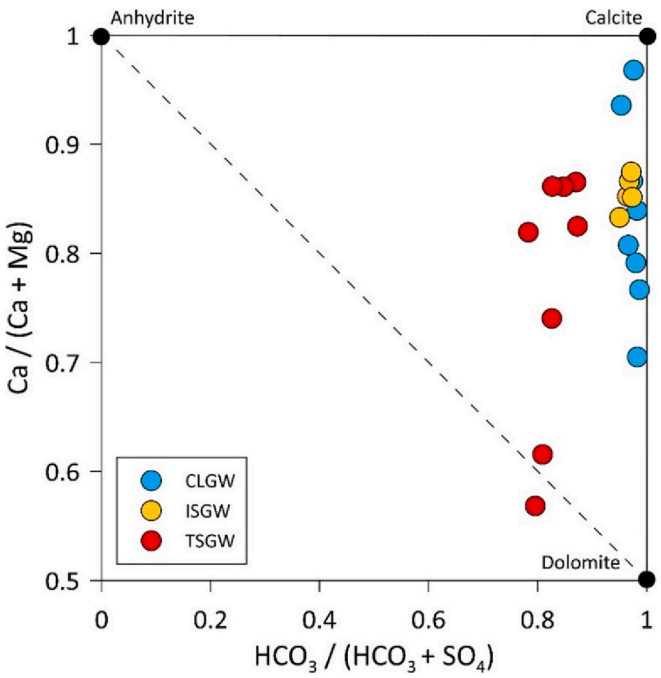

Fig. 5. Binary diagram: Ca/(Ca + Mg) vs $HCO_3/(HCO_3 + SO_4)$ (Apollaro et al., 2020).

processes. In addition, all waters are well-correlated ($R^2 = 0.94$) highlighting that the mixing processes between cold end-member and thermal deep one, evaporated in depth, can be occurred.

5.3. Tritium data

Based on the above-mentioned hydrogeochemical and isotopic considerations, different flowpaths can be supposed for the analysed groundwater. In order to estimate different residence times, the binary relationship between groundwater tritium and Cl^- contents was investigated. However, it did not show a linear correlation (Fig. S5). Based on the assumptions reported in the Methods section, the piston-flow model was applied only to the CLGW group, while the well-mixed reservoir model to ISGW and TSGW, according to the approach adopted by Apollaro et al. (2015, 2016). CLGW show tritium contents between 0.98 TU and 2.23, the two water samples of ISGW have tritium values of 1.7 TU and 2.2 TU respectively, and the tritium contents of TSGW are between 1.1 TU and 2.3 TU.

Based on the first above-mentioned model (i.e., piston-flow) with the uncertainties caused by the input functions of tritium data of rainwaters, a mean residence time of about 20 years has been estimated for CLGW. This residence time value indicates that these springs are discharged from a relatively young and shallow aquifer behaving as a piston-flow circuit of a high flow rate, as evidenced by their chemical composition too. Alternatively, for other groundwater groups by adopting the well-mixed reservoir model, the mean residence is greater than 100 years, with maximum values associated with TSGW. These values indicate that thermal waters are conditioned by longer circuits affecting the geothermal reservoir in depth, while ISGW is due to the mixing of meteoric water (same as CLGW) and thermal and brackish water uprising.

5.4. Reservoir temperature estimation

Considering the physical–chemical composition of the investigated groundwater and the geological-hydrogeological framework, the geothermal reservoir feeding the Contursi area thermal systems was expected to be hosted in carbonate-evaporitic rocks. Only TSGW type has been treated with geothermometric calculations, since these waters are the least affected by dilution and thus, they are the most representative of the thermal deep end-member. The SiO_2-quartz geothermometers (Truesdell, 1976; Fournier, 1977; Michard, 1979) show temperatures in the range 80–96 °C, while SiO_2-chalcedony geothermometers provide temperatures between 50 and 68 °C. The latter temperature range is slightly higher than the discharge temperature and therefore, quartz is likely the most phase controlling the dissolved silica contents in the studied area. The K-Mg geothermometers yields temperatures (from 75° to 96 °C) similar to those obtained with the SiO_2-quartz geothermometers. In previous studies (e.g., Apollaro et al., 2012; Pastorelli et al., 1999; Wang et al., 2015) these two geothermometers

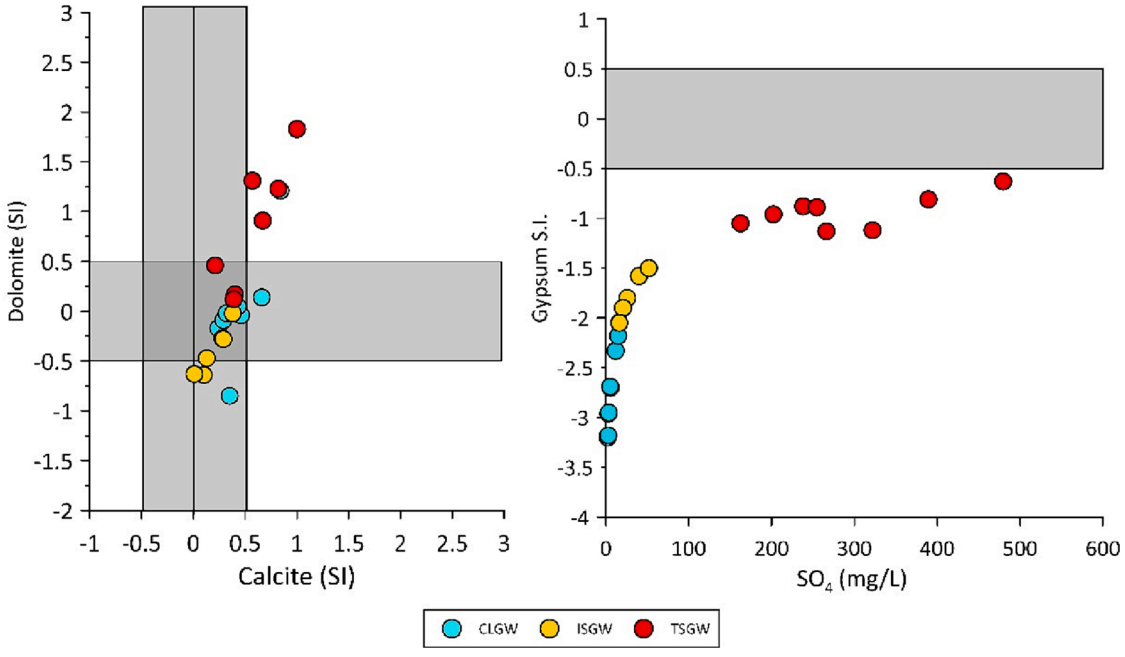

Fig. 6. A) Saturation indices: Calcite (SI) vs Dolomite (SI); b) Gypsum (SI) vs SO_4. Grey bars show ranges of equilibrium values (i.e., saturation state).

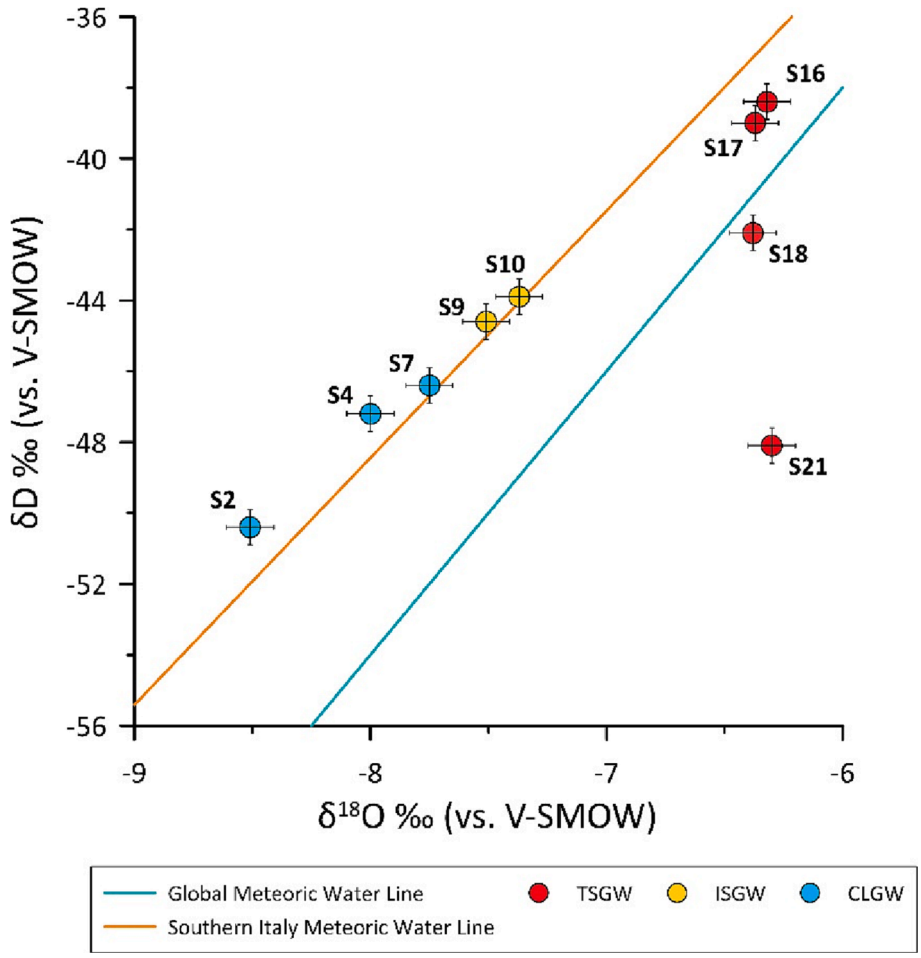

Fig. 7. Water stable isotopes diagram. $\delta^{18}O$ vs δD values of some samples from Sele river valley are shown with error bars. The Global Meteoric Water Line (Clark and Fritz, 2013), and the Southern Italy Meteoric Water Line (δD = 6.97 δ18O + 7.32; Longinelli and Selmo, 2003) are displayed with green, and orange lines, respectively.

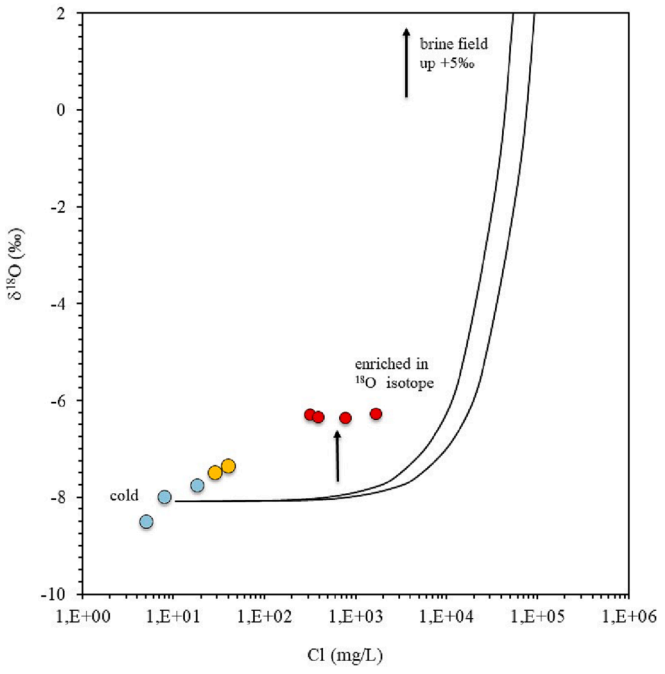

Fig. 8. The binary diagram displays the relationship between $\delta^{18}O$ and Cl^- contents (mg/L) of nine samples from the Sele river valley.

have been considered as the most suitable for low temperature carbonate-evaporitic systems. Considering all these results and excluding the higher values previously mentioned, a thermal reservoir temperature range of 75–95 °C can be considered representative for the investigated area. Taking into account the geothermometric estimations and the trend of geotherm proposed by Boncio et al., 2008, thermal reservoir can be estimated at the depth between 2 and 3 km.

5.5. $\delta^{34}S$ and $\delta^{18}O$ values in dissolved sulphate

The isotope composition of dissolved sulphate in groundwater has been analysed in order to constrain the sulphate origin in some water samples belonging to the ISGW and TSGW groups. The CLGW samples have not been analysed as they show low SO_4 values. The $\delta^{34}S$-SO_4 and $\delta^{18}O$-SO_4 values of the investigated groundwater samples fall into and very close to the field of evaporites (Fig. 10; Clark and Fritz, 1997; Paternoster et al., 2010; Petitta et al., 2011). Geological data indicate the presence of the Messinian Gessoso-Solfifera Formation at the top of the Apulian carbonates at a depth of about 4 km in "Acerno 001" well (Fig. 2). To ascertain that isotopic signature of studied waters is attributable to these evaporitic Messinian deposits, the $\delta^{34}S$-SO_4 values and SO_4 concentration of the water samples have been plotted together with mixing lines between rainwater and Messinian marine sulphate minerals (values from Boschetti et al., 2011a; Boschetti et al., 2011b; Vespasiano et al. 2021; Fig. 11). Three water samples (S9, S10 and S21) fall along the mixing lines, suggesting that the Messinian deposits are the mainly source of dissolved sulphate for the thermal systems of Contursi area.

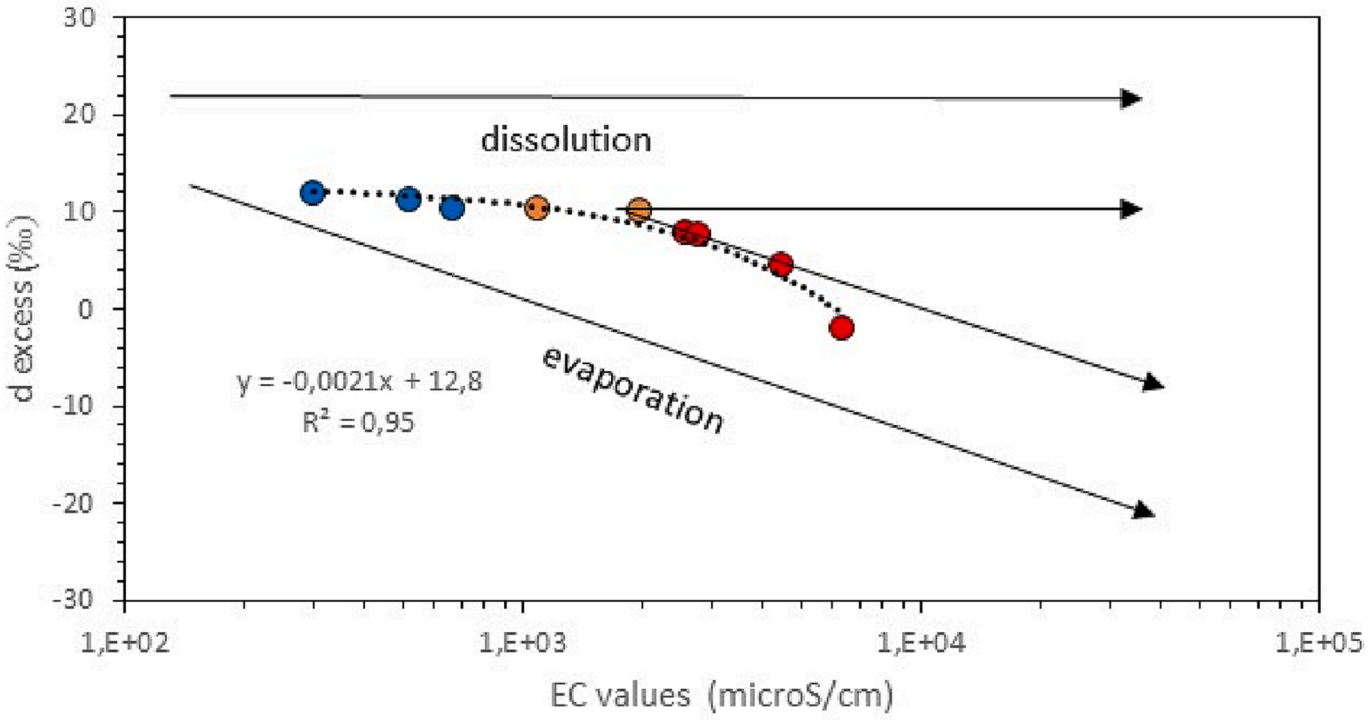

Fig. 9. Relationship between deuterium excess and EC (μS/cm) of nine samples from the Sele river valley.

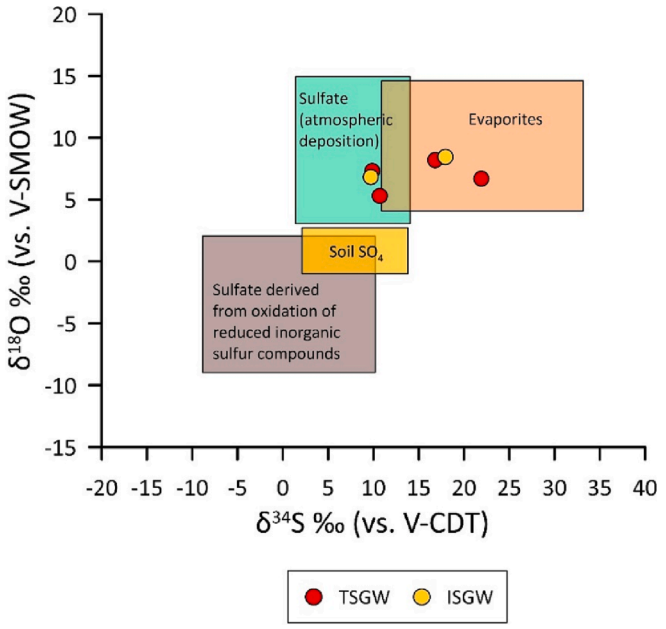

Fig. 10. Sulphate stable isotopes diagram (from Clark and Fritz, 1997). Isotope ranges for different potential sources of sulphate are displayed with rectangles. $\delta^{18}O\text{-}SO_4$ and $\delta^{34}S\text{-}SO_4$ isotopic values of some samples of ISGW and TSGW are shown.

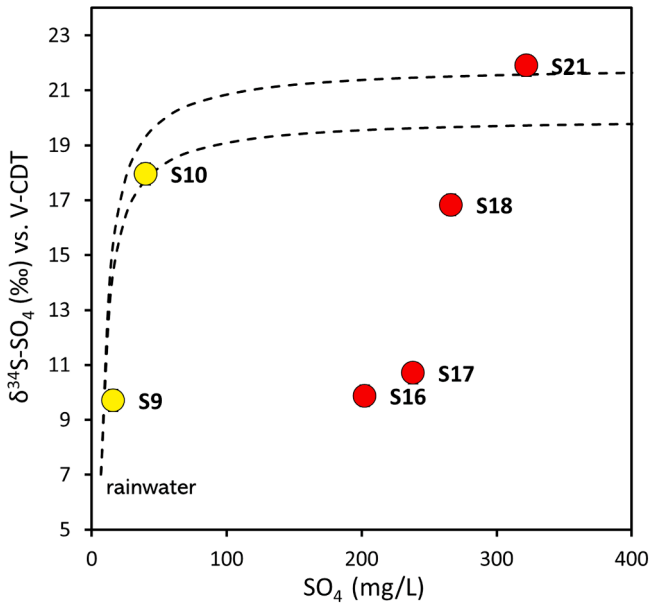

Fig. 11. $\delta^{34}S\text{-}SO_4$ (vs V-CDT) vs SO_4 concentration (mg/L) of groundwater samples are plotted together with mixing lines between rainwater and Messinian marine sulphate minerals.

Nevertheless, three samples (S16, S17 and S18) do not match the mixing model and show an ^{32}S-enrichment in the dissolved sulphate. Known that thermal waters are characterised by bubbling gases with high CO_2 and H_2S contents (Italiano et al., 2000; Minissale, 2004), it is possible that part of the H_2S of the gas phase is rapidly oxidized when it comes into contact with shallow meteoric water. The irreversible oxidation of H_2S, much faster kinetically than the reduction of sulphate to sulphide (Ohmoto and Rye, 1979), determines an ^{32}S-enrichment in the dissolved sulphate whose entity is function of the degree of oxidation in non-equilibrium condition as stated by Martinez Serrano et al. (1996). Therefore, for these samples the dissolved sulphate may be due to the contribution of oxidation of H_2S, and the Messinian deposits leaching at depth.

5.6. *Interpretative model of fluids flow*

This hydrogeochemical multi-approach allows to draw a hydro-geological model of the fluid circulation with the aid of cross-sections

(see Fig. 2). Hydrogeochemical and isotopic data (both stable and radioactive) indicate the existence of more complex and regional groundwater hydrodynamics for the ISGW and TSGW, which are characterized by longer and deeper flowpaths emerging in the inner zone of the Sele river valley. Instead, a local flow system with a shorter residence time of water is supposed for the CLGW shallow carbonate groundwater mostly emerging at the boundary of carbonate aquifers.

Besides, as shown in the geological schematic sections (Fig. 2), tectonic discontinuities (e.g., deep-seated faults) play a crucial role in the circulation, acting as pathways for the upward migration of deep contributions to reach the shallow regional aquifers that are totally recharged by meteoric infiltration (as stated by δD and $\delta^{18}O$ values). The mixing between deep-seated thermal fluids and colder shallow groundwater fed by regional carbonate aquifers occurs with different degree for ISGW and TSGW springs. Particularly, the latter ones show hydrogeochemical features directly connected with deep tectonic structures of the Contursi area (see Fig. 2). We speculate that deep inputs ascend from the Apulian Platform, where combinations of brine and or CO_2 mixtures are supposed (Duchi et al., 1995; Amoroso et al., 2017; De Landro et al., 2022), and crossing the Messinian deposits, they acquire the above-mentioned isotopic signature of evaporites. In the shallower portion of the crust (i.e., within the Carbonate tectonic unit), these mineralized fluids mix with fresh groundwater hosted in regional carbonate aquifers.

Our results are in line with recent geophysical studies carried out in this sector of Apennines that detected deep-seated fluid accumulation i.e., mixtures of brine and or CO_2 (Amoroso et al., 2014; Improta et al., 2014; Amoroso et al., 2017; De Landro et al., 2022). It is noteworthy also that De Landro et al., 2022 observed spatiotemporal seismic velocity changes that are caused by different mechanisms in the shallow and in the deep crust. In the shallower volume, they are associated with meteoric water recharge processes, and in the deeper volume they are related to pore pressure pulsations. Since previous works invoked overpressured fluids at depth as primary mechanism of interaction between fluid dynamic and earthquake triggering (Chiarabba et al., 2020; Chiodini et al., 2020), for future research the hydrogeochemical investigation in active seismic areas could be based on high-frequency and long-term multiparametric hydrogeochemical monitoring to quantify these pulsations as function of changes in mixing ratio between shallow groundwater and deep contributions.

6. Conclusion

In complex and active tectonic areas, the multi-component approach combining hydrogeochemistry to geo-structural setting and isotopic study is a powerful tool for analysing mixing and related processes between shallow groundwater and ascending deep fluids along main fault systems. The application of this tool to the Contursi area in the upper Sele river valley (southern Apennines, southern Italy) results to be appropriate to monitor this hydrogeochemical process, owing to its hydrogeological and geo-structural features. In fact, the study area is characterized by groundwater resources converging from shallow carbonate aquifers to several springs showing different geochemical signatures (e.g., degree of mineralization and thermalism), and by the presence of deep-seated tectonic discontinuities acting as preferential pathways for fluids upwelling.

A significant hydrogeochemical evolutionary trend from the Ca-Mg-HCO_3 hydrofacies to the Na-HCO_3-Cl one was found in the analysed groundwater samples. Thus, according to the geochemical composition as well as to the thermal trend and to the EC, three main groups of groundwater have been identified as follows: Cold and Low salinity Groundwater (CLGW), Intermediate Salinity Groundwater (ISGW), and Thermal and Saline Groundwater (TSGW). This classification was validated by stable isotopes ($\delta^{18}O$-δD). In fact, isotopic values of CLGW corresponding to the shallow end-member fall on the local meteoric water line (i.e., $\delta^{18}O$: from − 8.51 to − 7.75 ‰; δD: −50.4 to − 46.4 ‰), while ISGW and TSGW are characterized by isotopic signatures more enriched in heavy isotopes (i.e., $\delta^{18}O$: from − 7.51 to − 6.30 ‰; δD: −48.1 to − 38.4 ‰) attributed to the inflow of deep fluids which have undergone natural processes modifying the pristine isotopic signature.

Therefore, CLGW chemistry is clearly related to carbonate rocks (calcite and dolomite)-water interaction. In contrast, for ISGW and TSGW an additional contribution from evaporitic rocks can be proposed as shown by chemical composition, SI values (gypsum and anhydrite) and sulphur isotopic signature of dissolved sulphate, whose values are associated with the evaporitic Messinian Gessoso-Solfifera Formation.

Our geo-structural review provided a structural sketch down to a depth of approximately 5 km. The geological cross-sections highlighted the presence of deep-seated normal faults which could represent the best network of pathways for deep fluids migration towards the surface allowing the mixing between deep and shallow end-members.

Additionally, through the application of two models (i.e., the piston-flow and well-mixed reservoir) based on tritium isotope, deeper and longer circuits have been pointed out for TSGW flowpaths. Also, by selecting geothermometers for medium–low geothermal systems, the equilibrium reservoir temperature of deep contributions between 75 and 96 °C was extrapolated for springs where evidence of significant deep contributions was found. Hence, applying the geothermal gradient of the study area, an estimation of depth of fluids reservoir at about 3 km was inferred.

Moreover, our results agree with recent geodetical and seismological studies in the selected area that reported an intensely fractured deep fluid-saturated volume of the crust. The same studies shed light on the spatiotemporal evolution of pore pressure pulsations at depth in highly sensitive fault system zones. At the same time, in the shallow crust, transient deformations were attributable to phases of recharge of wide aquifers. Consequently, recording changes in hydrogeological mixing ratio by long-lasting hydrogeochemical multi-component approach could be crucial to analyse and discern both the pore pressure pulsations in the deep crust and hydrogeological variations in the shallow crust.

CRediT authorship contribution statement

Francesca Gori: Conceptualization, Methodology, Investigation, Formal analysis, Software, Data curation, Writing – original draft. **Michele Paternoster:** Conceptualization, Methodology, Investigation, Data curation, Validation, Writing – original draft, Writing – review & editing. **Maurizio Barbieri:** Conceptualization, Methodology, Validation, Supervision. **Dario Buttitta:** Methodology, Investigation. **Antonio Caracausi:** Conceptualization, Methodology, Investigation, Validation, Supervision. **Fabrizio Parente:** Methodology, Investigation, Software, Data curation, Writing – original draft. **Attilio Sulli:** Conceptualization, Methodology, Validation, Supervision, Writing – review & editing. **Marco Petitta:** Conceptualization, Methodology, Supervision, Project administration, Writing – review & editing.

Declaration of Competing Interest

The authors declare that they have no known competing financial interests or personal relationships that could have appeared to influence the work reported in this paper.

Data availability

All data are freely available

Acknowledgements

We acknowledge institutional financial support from Sapienza University of Rome, Italy: Granted Sapienza Project 2020: “Hydrogeochemical seismic precursors in the Apennines” PI: Carlo Doglioni; and Granted Sapienza Project 2021: “Monitoraggio intensivo

multiparametrico di dati idrogeologici e idrogeochimici correlabili alla sismicità in Appennino Centro-Meridionale" PI: Marco Petitta). We thank the water company "ASIS Salernitana Reti ed Impianti SpA" and the thermal spas of Contursi Terme and Bagni di Contursi villages for allowing us access and the collection of groundwater samples. Finally, we thank the anonymous reviewers for their constructive comments and suggestions that allowed us to significantly improve the manuscript form and content.

Appendix A. Supplementary data

Supplementary data to this article can be found online at https://doi.org/10.1016/j.jhydrol.2023.129258.

References

Amoroso, O., Ascione, A., Mazzoli, S., Virieux, J., Zollo, A., 2014. Seismic imaging of a fluid storage in the actively extending Apennine mountain belt, southern Italy. Geophys. Res. Lett. 41 (11), 3802–3809.

Amoroso, O., Russo, G., De Landro, G., Zollo, A., Garambois, S., Mazzoli, S., Parente, M., Virieux, J., 2017. From velocity and attenuation tomography to rock physical modeling: Inferences on fluid-driven earthquake processes at the Irpinia fault system in southern Italy. Geophys. Res. Lett. 44 (13), 6752–6760.

Andreo, B., Gil-Márquez, J.M., Mudarra, M., Linares, L., Carrasco, F., 2016. Hypothesis on the hydrogeological context of wetland areas and springs related to evaporitic karst aquifers (Málaga, Córdoba and Jaén provinces, Southern Spain). Environ. Earth Sci. 75 (9), 1–19.

Apollaro, C., Dotsika, E., Marini, L., Barca, D., Bloise, A., De Rosa, R., Doveri, M., Lelli, M., Muto, F., 2012. Chemical and isotopic characterization of the thermomineral water of Terme Sibarite springs (Northern Calabria, Italy). Geochem. J. 46 (2), 117–129.

Apollaro, C., Vespasiano, G., De Rosa, R., Marini, L., 2015. Use of mean residence time and flowrate of thermal waters to evaluate the volume of reservoir water contributing to the natural discharge and the related geothermal reservoir volume. Application to Northern Thailand hot springs. Geothermics 58, 62–74.

Apollaro, C., Vespasiano, G., Muto, F., De Rosa, R., Barca, D., Marini, L., 2016. Use of mean residence time of water, flowrate, and equilibrium temperature indicated by water geothermometers to rank geothermal resources. Application to the thermal water circuits of Northern Calabria. J. Volcanol. Geotherm. Res. 328, 147–158.

Apollaro, C., Caracausi, A., Paternoster, M., Randazzo, P., Aiuppa, A., De Rosa, R., Fuoco, I., Mongelli, G., Muto, F., Vanni, E., Vespasiano, G., 2020. Fluid geochemistry in a low-enthalpy geothermal field along a sector of southern Apennines chain (Italy). J. Geochem. Explor. 219, 106618.

Appelo, C.A.J., Postma, D., 2005. Geochemistry. Groundwater and pollution 536.

Arnórsson, S., Gunnlaugsson, E., Svavarsson, H., 1983. The chemistry of geothermal waters in Iceland. III. Chemical geothermometry in geothermal investigations. Geochim. Cosmochim. Acta 47 (3), 567–577.

Ascione, A., Nardò, S., Mazzoli, S., 2020. The MS 6.9, 1980 Irpinia Earthquake from the basement to the surface: a review of tectonic geomorphology and geophysical constraints, and new data on postseismic deformation. Geosciences 10 (12), 493.

Baird R.B., Eaton A.D., Rice, E.W., 2017. Standard methods for examination of water and wastewater, 23rd edn. American Public Health Association (APHA), American Water Works Association (AWWA), Water Environment Federation (WEF), Washington DC.

Barberio, M.D., Gori, F., Barbieri, M., Boschetti, T., Caracausi, A., Cardello, G.L., Petitta, M., 2021. Understanding the origin and mixing of deep fluids in shallow aquifers and possible implications for crustal deformation studies: San Vittorino plain. Central Apennines. Appl. Sci. 11 (4), 1353.

Barbieri, M., Boschetti, T., Barberio, M.D., Billi, A., Franchini, S., Iacumin, P., Selmo, E., Petitta, M., 2020. Tracing deep fluid source contribution to groundwater in an active seismic area (central Italy): A combined geothermometric and isotopic (δ13C) perspective. J. Hydrol. 582, 124495.

Battistel, M., Hurwitz, S., Evans, W., Barbieri, M., 2014. Multicomponent geothermometry applied to a medium-low enthalpy carbonate-evaporite geothermal reservoir. Energy Procedia 59, 359–365.

Battistel, M., Hurwitz, S., Evans, W.C., Barbieri, M., 2016. The chemistry and isotopic composition of waters in the low-enthalpy geothermal system of Cimino-Vico Volcanic District. Italy. J. Volcanol. Geotherm. Res. 328, 222–229.

Bernard, P., Zollo, A., 1989. The Irpinia (Italy) 1980 earthquake: detailed analysis of a complex normal faulting. J. Geophys. Res. Solid Earth 94 (B2), 1631–1647.

Boni, C., Bono, P., Capelli, G., 1986. Schema Idrogeologico dell'Italia Centrale. Mem. Soc. Geol. It. 991–1012.

Boschetti, T., Toscani, L., Shouakar-Stash, O., Iacumin, P., Venturelli, G., Mucchino, C., Frape, S.K., 2011a. Salt waters of the Northern Apennine Foredeep Basin (Italy): origin and evolution. Aquat. Geochem. 17 (1), 71–108.

Boschetti, T., Cortecci, G., Toscani, L., Iacumin, P., 2011b. Sulfur and oxygen isotope compositions of Upper Triassic sulfates from Northern Apennines (Italy): palaeogeographic and hydrogeochemical implications. Geol. Acta 9, 129–147.

Budetta, P., Celico, P., Corniello, A., De Riso, R., Ducci, D., Nicotera, P., 1988. Carta idrogeologica del F. 186 (S. Angelo dei Lombardi). Memoria illustrativa. Mem. Soc. Geol. It. 41, 1029–1038.

Capaccioni, B., Didero, M., Paletta, C., Salvadori, P., 2001. Hydrogeochemistry of groundwaters from carbonate formations with basal gypsiferous layers: an example from the Mt Catria–Mt Nerone ridge (Northern Appennines, Italy). J. Hydrol. 253 (1–4), 14–26.

Capecchiacci, F., Tassi, F., Vaselli, O., Bicocchi, G., Cabassi, J., Giannini, L., Nisi, B., Chiocciora, G., 2015. A combined geochemical and isotopic study of the fluids discharged from the Montecatini thermal system (NW Tuscany, Italy). Appl. Geochem. 59, 33–46.

Celico, P.B., 1983. Idrogeologia dei massicci carbonatici, delle piane quaternarie e delle aree vulcaniche dell'Italia centro-meridionale: Marche e Lazio meridionali, Abruzzo. Molise e Campania, Cassa per il Mezzogiorno.

Celico, P., Civita, M., 1976. Sulla tettonica del Massiccio del Cervialto (Campania) e le implicazioni idrogeologiche ad essa connesse. Boll. Soc. Natur. in Napoli 85, 555–580.

Celico, P., De Gennaro, M., Ghiara, M.R., Stanzione, D., 1979. Le sorgenti termominerali della valle del Sele (SA): indagini strutturali, idrogeologiche e Geochimiche. Rend. Soc. Ital. Mineral. Petrol. 31, 389–409.

Celico, P., Guadagno, F.M., Luise, G., Tescione, M., Vallario, A., 1987. Idrogeologia del Monte Polveracchio – Monte Raione (Monti Picentini - Campania). Mem. Soc. Geol. It. 37, 341–362.

Celico, F., Petrella, E., Celico, P., 2006. Hydrogeological behaviour of some fault zones in a carbonate aquifer of Southern Italy: an experimentally based model. Terra Nova 18 (5), 308–313.

Chen, Z., Goldscheider, N., 2014. Modeling spatially and temporally varied hydraulic behavior of a folded karst system with dominant conduit drainage at catchment scale, Hochifen-Gottesacker. Alps. J. Hydrol. 514, 41–52.

Chiarabba, C., Buttinelli, M., Cattaneo, M., De Gori, P., 2020. Large earthquakes driven by fluid overpressure: The Apennines normal faulting system case. Tectonics 39 (4), e2019.

Chiocchini, U., Castaldi, F., Barbieri, M., Eulilli, V., 2010. A stratigraphic and geophysical approach to studying the deep-circulating groundwater and thermal springs, and their recharge areas, in Cimini Mountains-Viterbo area, central Italy. Hydrogeol. J. 18, 1319–1341.

Chiodini, G., Frondini, F., Marini, L., 1995a. Theoretical geothermometers and PCO2 indicators for aqueous solutions coming from hydrothermal systems of medium-low temperature hosted in carbonate-evaporite rocks. Application to the thermal springs of the Etruscan Swell, Italy. Appl. Geochem. 10 (3), 337–346.

Chiodini, G., Frondini, F., Ponziani, F., 1995b. Deep structures and carbon dioxide degassing in central Italy. Geothermics 24 (1), 81–94.

Chiodini, G., Cardellini, C., Amato, A., Boschi, E., Caliro, S., Frondini, F., Ventura, G., 2004. Carbon dioxide Earth degassing and seismogenesis in central and southern Italy. Geophys. Res. Lett. 31 (7).

Chiodini, G., Cardellini, C., Di Luccio, F., Selva, J., Frondini, F., Caliro, S., Rosiello, A., Beddini, G., Ventura, G., 2020. Correlation between tectonic CO_2 Earth degassing and seismicity is revealed by a 10-year record in the Apennines, Italy. Sci. Adv. 6 (35), eabc2938.

Ciarcia, S., Vitale, S., Di Staso, A., Iannace, A., Mazzoli, S., Torre, M., 2009. Stratigraphy and tectonics of an Internal Unit of the southern Apennines: implications for the geodynamic evolution of the peri-Tyrrhenian mountain belt. Terra Nova 21 (2), 88–96.

Clark, I.D., Fritz, P., 1997. Environmental Isotopes in Hydrogeology. Lewis Publishers, New York.

Clark, I.D., Fritz, P., 2013. Environmental isotopes in hydrogeology. CRC Press.

Clayton, R.N., Steiner, A., 1975. Oxygen isotope studies of the geothermal system at Wairakei. New Zealand. Geochim. Cosmochim. Acta 39 (8), 1179–1186.

Cook, P.G., 2003. A guide to regional groundwater flow in fractured rock aquifers. Seaview Press, Henley Beach, South Australia, p. 151.

Coppola, L., Pescatore, T., 1989. Lineamenti di neotettonica dei Monti Terminio-Tuoro, Cervialto e Marzano (Appennino meridionale). Bollettino Società Geologica Italiana 108 (1), 105–119.

Corniello, A., Ducci, D., Aquino, A., 2010. Hydrogeological map of the Monti Picentini Regional Park (southern Italy) at 1: 50,000 scale. Bollettino Geofisica Teorica ed Applicata 51 (4).

Cotecchia, V., 1986. Ground deformation and slope instability produced by the earthquake slope of 23 November 1980 in Campania and Basilicata. Geol. Appl. Idrogeol. 21, 31–100.

De Landro, G., Amoroso, O., Russo, G., D'Agostino, N., Esposito, R., Emolo, A., Zollo, A., 2022. Decade-long monitoring of seismic velocity changes at the Irpinia fault system (southern Italy) reveals pore pressure pulsations. Sci. Rep. 12 (1), 1–9.

De Matteis, R., Matrullo, E., Rivera, L., Stabile, T.A., Pasquale, G., Zollo, A., 2012. Fault delineation and regional stress direction from the analysis of background microseismicity in the southern Apennines, Italy. Bulletin of the Seismological Society of America 102 (4), 1899–1907.

De Vries, J.J., Simmers, I., 2002. Groundwater recharge: an overview of processes and challenges. Hydrogeol. J. 10 (1), 5–17.

Deutsch, W.J., 2020. Groundwater Geochemistry: Fundamentals And Applications To Contamination. CRC Press.

Di Nocera S., Iannace A., Torre M., Basso C., Caiazzo C., Ciarcia S., Cinque A., Gasparrini M., Matano F., Mazzoli S., Mitrano T., Pagliaro S. Parente M., 2016. Note illustrative della Carta Geologica d'Italia alla scala 1: 50.000, foglio 468 Eboli. ISPRA Istituto Superiore per la Protezione e la Ricerca Ambientale, Servizio Geologico d'Italia.

Doglioni, C., 1991. A proposal for the kinematic modelling of W-dipping subductions-possible applications to the Tyrrhenian-Apennines system. Terra Nova 3 (4), 423–434.

Doglioni, C., 1995. Geological remarks on the relationships between extension and convergent geodynamic settings. Tectonophysics 252 (1–4), 253–267.

Doglioni, C., Barba, S., Carminati, E., Riguzzi, F., 2014. Fault on–off versus coseismic fluids reaction. Geosci. Front. 5 (6), 767–780.
Drever, J.I., 1997. The geochemistry of natural waters: surface and groundwater environments, 3rd edn. Prentice Hall, Upper Saddle River.
Duchi, V., Minissale, A., Vaselli, O., Ancillotti, M., 1995. Hydrogeochemistry of the Campania region in southern Italy. J. Volcanol. Geotherm. Res. 67 (4), 313–328.
Faccenna, C., Becker, T.W., Lucente, F.P., Jolivet, L., Rossetti, F., 2001. History of subduction and back arc extension in the Central Mediterranean. Geophys. J. Int. 145 (3), 809–820.
Fouillac, C., Michard, G., 1981. Sodium/lithium ratio in water applied to geothermometry of geothermal reservoirs. Geothermics 10 (1), 55–70.
Fournier, R.O., 1977. Chemical geothermometers and mixing models for geothermal systems. Geothermics 5 (1–4), 41–50.
Fournier, R.O., 1979. A revised equation for the Na/K geothermometer. Transactions of the Geothermal Resources Council 3, 221–224.
Fournier, R.O., Potter, I., R. w., 1979. Magnesium correction to the Na K Ca chemical geothermometer. Geochim. Cosmochim. Acta 43 (9), 1543–1550.
Fournier, R.O., Truesdell, A.H., 1973. An empirical Na K Ca geothermometer for natural waters. Geochim. Cosmochim. Acta 37 (5), 1255–1275.
Freeze, R.A., Cherry, J.A., 1979. Groundwater. PrenticeHall, Englewood, Cliffs, New Jersey, p. 604.
Frondini, F., 2008. Geochemistry of regional aquifer systems hosted by carbonate-evaporite formations in Umbria and southern Tuscany (central Italy). Appl. Geochem. 23 (8), 2091–2104.
Ghiara, M.R., Stanzione, D., Petti, C., 1994. Chemical and isotope characteristics of the deep waters of the high valley of the River Sele (Italy); correlations between geochemical parameters and seismic activity. Bollettino Società Geologica Italiana 113 (3), 521–537.
Giggenbach, W.F., 1988. Geothermal solute equilibria. derivation of Na-K-Mg-Ca geoindicators. Geochim. Cosmochim. Acta 52 (12), 2749–2765.
Giggenbach, W.F., 1992. Isotopic shifts in waters from geothermal and volcanic systems along convergent plate boundaries and their origin. Earth Planet. Sci. Lett. 113 (4), 495–510.
Gil-Márquez, J.M., Barberá, J.A., Andreo, B., Mudarra, M., 2017. Hydrological and geochemical processes constraining groundwater salinity in wetland areas related to evaporitic (karst) systems. A case study from Southern Spain. J. Hydrol. 544, 538–554.
Goldscheider, N., Mádl-Szőnyi, J., Erőss, A., Schill, E., 2010. Thermal water resources in carbonate rock aquifers. Hydrogeol. J. 18 (6), 1303–1318.
Gori, F., Barberio, M.D., 2022. Hydrogeochemical changes before and during the 2019 Benevento seismic swarm in central-southern Italy. J. Hydrol. 604, 127250.
Hoefs, J., 2009. Stable isotope geochemistry, 6th ed. Springer.
Holser, W.T., 2018. Trace elements and isotopes in evaporites. In: Marine Minerals. De Gruyter, pp. 295–346.
IAEA/WMO, 2013. Global network of isotopes in precipitation. The GNIP database. (Accessible at: http://www.iaea.org/water).
Improta, L., De Gori, P., Chiarabba, C., 2014. New insights into crustal structure, Cenozoic magmatism, CO_2 degassing, and seismogenesis in the southern Apennines and Irpinia region from local earthquake tomography. J. Geophys. Res. Solid Earth 119 (11), 8283–8311.
Italiano, F., Martelli, M., Martinelli, G., Nuccio, P.M., 2000. Geochemical evidence of melt intrusions along lithospheric faults of the Southern Apennines, Italy: geodynamic and seismogenic implications. J. Geophys. Res. Solid Earth 105 (B6), 13569–13578.
Karolytė, R., Serno, S., Johnson, G., Gilfillan, S.M., 2017. The influence of oxygen isotope exchange between CO_2 and H_2O in natural CO_2-rich spring waters: Implications for geothermometry. Appl. Geochem. 84, 173–186.
Kharaka, Y.K., Hanor, J.S., 2003. Deep fluids in the continents: I. Sedimentary basins. Treat. Geochem. 5, 605.
Langelier, W.F., Ludwig, H.F., 1942. Graphical methods for indicating the mineral character of natural waters. Journal (American water works association) 34 (3), 335–352.
Longinelli, A., Selmo, E., 2003. Isotopic composition of precipitation in Italy: a first overall map. J. Hydrol. 270 (1–2), 75–88.
Ma, R., Wang, Y., Sun, Z., Zheng, C., Ma, T., Prommer, H., 2011. Geochemical evolution of groundwater in carbonate aquifers in Taiyuan, northern China. Appl. Geochem. 26 (5), 884–897.
Maćkiewicz, A., Ratajczak, W., 1993. Principal components analysis (PCA). Comput. Geosci. 19 (3), 303–342.
Malinverno, A., Ryan, W.B., 1986. Extension in the Tyrrhenian Sea and shortening in the Apennines as result of arc migration driven by sinking of the lithosphere. Tectonics 5 (2), 227–245.
Marini, L., Chiodini, G., Cioni, R., 1986. New geothermometers for carbonate—evaporite geothermal reservoirs. Geothermics 15 (1), 77–86.
Martínez Serrano, R.G., Jacquier, B., Arnold, M., 1996. The δ34S composition of sulfates and sulfides at the Los Humeros geothermal system, Mexico and their application to physicochemical fluid evolution. J. Volcanol. Geotherm. Res. 73, 99–118.
Matsuhisa, Y., Goldsmith, J.R., Clayton, R.N., 1979. Oxygen isotopic fractionation in the system quartz-albite-anorthite-water. Geochim. Cosmochim. Acta 43 (7), 1131–1140.
Matthess, G., 1982. The Properties Of Groundwater. Wiley, New York, p. 498.
McMahon, P.B., 2012. Use of classes based on redox and groundwater age to characterize the susceptibility of principal aquifers to changes in nitrate concentrations. 1991 to 2010: U.S. Geological Survey Scientific Investigations Report 2012–5220.
Merlini, S., Mostardini, F., 1986. Appennino centro-meridionale: sezioni geologiche e proposta di modello strutturale. Geologia dell'Italia centrale. Congresso nazionale. 73, 147–149.
Michard, G., 1979. Géothermomètres chimiques. Bull de BRGM III (2), 183–189.
Minissale, A., 1991. Thermal springs in Italy: their relation to recent tectonics. Appl. Geochem. 6 (2), 201–212.
Minissale, A., 2004. Origin, transport and discharge of CO_2 in central Italy. Earth-Sci. Rev. 66 (1–2), 8–141.
Minissale, A., Donato, A., Procesi, M., Giammanco, S., Pizzino, L., 2016. Dati e Carte geochimiche del Mezzogiorno d'Italia.
Montanari, D., Minissale, A., Doveri, M., Gola, G., Trumpy, E., Santilano, A., Manzella, A., 2017. Geothermal resources within carbonate reservoirs in western Sicily (Italy): A review. Earth-Sci. Rev. 169, 180–201.
Nollet, L.M.L., 2007. Handbook of Water Analysis 2nd Ed, The Journal of Nutrition, Health Aging.
Ohmoto, H. and Rye, R.O., 1979. Isotopes of sulfur and carbon. In: H.L. Barnes (Editor), Geochemistry of Hydrothermal Ore Deposits, 2nd edition. Publisher? New York. ch. IO: 509–567.
Ortolani, F., 1975. Assetto strutturale dei Monti Picentini, della Valle del Sele e del Gruppo di Monte Marzano – Monte Ogna (Appennino Meridionale). Implicazioni idrogeologiche. Boll. Soc. Geol. It. 94, 209–230.
Panichi, C., Tongiorgi, E., 1975. Carbon isotopic composition of CO_2 from springs, fumaroles, mofettes, and travertines of central and southern Italy. Proc. 2nd U.N. Symp. Devel. Use Geothermal Resources, San Francisco 1, 815–825.
Parkhurst, D.L., Appelo, C.A.J., 2013. Description of input and examples for PHREEQC version 3—a computer program for speciation, batch-reaction, one-dimensional transport, and inverse geochemical calculations. US Geol. Survey Techniq. Methods 6 (A43), 497.
Pastorelli, S., Marini, L., Hunziker, J.C., 1999. Water chemistry and isotope composition of the Acquarossa thermal system, Ticino, Switzerland. Geothermics 28 (1), 75–93.
Patacca, E., Scandone, P., 2007. Geology of the southern Apennines. Bollettino Società Geol. Ital. 7, 75–119.
Paternoster, M., Parisi, S., Caracausi, A., Favara, R., Mongelli, G., 2010. Groundwaters of Mt. Vulture volcano, southern Italy: chemistry and sulfur isotope composition of dissolved sulfate. Geochem. J. 44 (2), 125–135.
Paternoster, M., Oggiano, G., Sinisi, R., Caracausi, A., Mongelli, G., 2017. Geochemistry of two contrasting deep fluids in the Sardinia microplate (western Mediterranean): Relationships with tectonics and heat sources. J. Volcanol. Geotherm. Res. 336, 108–117.
Petitta, M., Primavera, P., Tuccimei, P., Aravena, R., 2011. Interaction between deep and shallow groundwater systems in areas affected by Quaternary tectonics (Central Italy): a geochemical and isotope approach. Environ. Earth Sci. 63 (1), 11–30.
Pierdominici, S., Mariucci, M.T., Montone, P., 2011. A study to constrain the geometry of an active fault in southern Italy through borehole breakouts and downhole logs. J. Geodyn. 52 (3–4), 279–289.
Qiu, X., Wang, Y., Wang, Z., Regenauer-Lieb, K., Zhang, K., Liu, J., 2018. Determining the origin, circulation path and residence time of geothermal groundwater using multiple isotopic techniques in the Heyuan Fault Zone of Southern China. J. Hydrol. 567, 339–350.
Richet, P., Bottinga, Y., Javoy, M., 1977. A review of hydrogen, carbon, nitrogen, oxygen, sulphur, and chlorine stable isotope fractionation among gaseous molecules. Annu. Rev. Earth Planet. Sci. 5 (1), 65–110.
Sanford, W., 2011. Calibration of models using groundwater age. Hydrogeol. J. 19 (1), 13–16.
Sharp, Z. (2017). Principles of stable isotope geochemistry.
Shevenell, L., Goff, F., 1995. The use of tritium in groundwater to determine fluid mean residence times of Valles caldera hydrothermal fluids, New Mexico. USA. J. Volcanol. Geotherm. Res. 67 (1–3), 187–205.
Shiner, P., Beccacini, A., Mazzoli, S., 2004. Thin-skinned versus thick-skinned structural models for Apulian carbonate reservoirs: constraints from the Val d'Agri Fields, S Apennines. Italy. Mar. Pet. Geol. 21 (7), 805–827.
Sibson, R.H., Moore, J.M.M., Rankin, A.H., 1975. Seismic pumping—a hydrothermal fluid transport mechanism. Journal of the Geological Society 131 (6), 653–659.
Slejko, D., Peruzza, L., Rebez, A., 1998. Seismic hazard maps of Italy.
Smeraglia, L., Bernasconi, S.M., Berra, F., Billi, A., Boschi, C., Caracausi, A., Carminati, E., Castorina, F., Doglioni, C., Italiano, F., Rizzo, L.A., Uysal, I.T., Zhao, J. X., 2018. Crustal-scale fluid circulation and co-seismic shallow comb-veining along the longest normal fault of the central Apennines. Italy. Earth Planet. Sci. Lett. 498, 152–168.
Smeraglia, L., Aldega, L., Bernasconi, S.M., Billi, A., Boschi, C., Caracausi, A., Carminati, E., Franchini, S., Rizzo, A.L., Rossetti, F., Vignaroli, G., 2020. The role of trapped fluids during the development and deformation of a carbonate/shale intra-wedge tectonic mélange (Mt. Massico, Southern Apennines, Italy). J. Struct. Geol. 138, 104086.
Tarquini, S., Isola, I., Favalli, M., Mazzarini, F., Bisson, M., Pareschi, M.T., Boschi, E., 2007. TINITALY/01: a new triangular irregular network of Italy. Ann, Geophys.
Toscani, L., Boschetti, T., Maffini, M., Barbieri, M., Mucchino, C., 2007. The groundwaters of Fontevivo (Parma Province, Italy): redox processes and mixing with brine waters. Geochem.: Explor. Environ. Anal. 7 (1), 23–40.
Toth, J., 1995. Hydraulic continuity in large sedimentary basins. Hydrogeol. J. 3 (4), 4–16.
Trippetta, F., Collettini, C., Barchi, M.R., Lupattelli, A., Mirabella, F., 2013. A multidisciplinary study of a natural example of a CO_2 geological reservoir in central Italy. Int. J. Greenh. Gas Control. 12, 72–83.

Truesdell, A. H. 1976. Summary of section III-geochemical techniques in exploration. In Proc. 2nd UN Symp. on the Development and Use of Geothermal Resources (Vol. 1, pp. 1iii-1xxix).

Valoroso, L., Improta, L., De Gori, P., Chiarabba, C., 2011. Upper crustal structure, seismicity and pore pressure variations in an extensional seismic belt through 3-D and 4-D VP and VP/VS models: The example of the Val d'Agri area (southern Italy). J. Geophys. Res. Solid Earth 116 (B7).

Vannoli, P., Martinelli, G., Valensise, G., 2021. The seismotectonic significance of geofluids in Italy. Front. Earth Sci. 9, 25.

Vespasiano, G., Marini, L., Muto, F., Auqué, L.F., Cipriani, M., De Rosa, R., Critelli, S., Gimeno, M.J., Blasco, M., Dotsika, E., Apollaro, C., 2021. Chemical, isotopic and geotectonic relations of the warm and cold waters of the Cotronei (Ponte Coniglio), Bruciarello and Repole thermal areas (Calabria-Southern Italy). Geothermics 96, 102228.

Vitale, S., Ciarcia, S., 2018. Tectono-stratigraphic setting of the Campania region (southern Italy). J. Maps 14 (2), 9–21.

Wang, H.Y., Guo, H.M., Xiu, W., Bauer, J., Sun, G.X., Tang, X.H., Norra, S., 2019. Indications that weathering of evaporite minerals affects groundwater salinity and As mobilization in aquifers of the northwestern Hetao Basin. China. Appl. Geochem. 109, 104416.

Wang, B., Jin, M., Nimmo, J.R., Yang, L., Wang, W., 2008. Estimating groundwater recharge in Hebei Plain, China under varying land use practices using tritium and bromide tracers. J Hydrol. 356 (1–2), 209–222.

Wang, J., Jin, M., Jia, B., Kang, F., 2015. Hydrochemical characteristics and geothermometry applications of thermal groundwater in northern Jinan, Shandong, China. Geothermics 57, 185–195.

Wasowski, J., Pierri, V., Pierri, P., Capolongo, D., 2002. Factors controlling seismic susceptibility of the Sele valley slopes: the case of the 1980 Irpinia earthquake re-examined. Surv. Geophys. 23 (6), 563–593.

Yan, Q., Gao, Z., Ni, S., Shi, Z., Yin, G., 2013. Evolution of isotopic composition and deuterium excess of brines in the Sichuan Basin. China. Chinese J. Chem. 32 (1), 69–77.

Yang, P., Luo, D., Hong, A., Ham, B., Xie, S., Ming, X., Wang, Z., Pang, Z., 2019. Hydrogeochemistry and geothermometry of the carbonate-evaporite aquifers controlled by deep-seated faults using major ions and environmental isotopes. J. Hydrol. 579, 124116.